nature immunology

Article

https://doi.org/10.1038/s41590-023-01571-5

CTLA-4 tail fusion enhances CAR-T antitumor immunity

Received: 11 July 2022

Accepted: 21 June 2023

Published online: 27 July 2023

Check for updates

Xiaoyu Zhou[1,2,3,13], Hanbing Cao[1,2,3,13], Shao-Yu Fang[1,2,3], Ryan D. Chow[1,2,3,4,5,6], Kaiyuan Tang[1,2,3,4], Medha Majety[1,2,3,7], Meizhu Bai[1,2,3], Matthew B. Dong[1,2,3,5,6,8], Paul A. Renauer[1,2,3,4], Xingbo Shang[2,3,9], Kazushi Suzuki[1,2,3], Andre Levchenko[2,3,9] & Sidi Chen[1,2,3,4,5,8,10,11,12]

Chimeric antigen receptor (CAR)-T cells are powerful therapeutics; however, their efficacy is often hindered by critical hurdles. Here utilizing the endocytic feature of the cytotoxic T-lymphocyte-associated antigen-4 (CTLA-4) cytoplasmic tail, we reprogram CAR function and substantially enhance CAR-T efficacy in vivo. CAR-T cells with monomeric, duplex or triplex CTLA-4 cytoplasmic tails (CCTs) fused to the C terminus of CAR exhibit a progressive increase in cytotoxicity under repeated stimulation, accompanied by reduced activation and production of proinflammatory cytokines. Further characterization reveals that CARs with increasing CCT fusion show a progressively lower surface expression, regulated by their constant endocytosis, recycling and degradation under steady state. The molecular dynamics of reengineered CAR with CCT fusion results in reduced CAR-mediated trogocytosis, loss of tumor antigen and improved CAR-T survival. CARs with either monomeric (CAR-1CCT) or duplex CCTs (CAR-2CCT) have superior antitumor efficacy in a relapsed leukemia model. Single-cell RNA sequencing and flow cytometry analysis reveal that CAR-2CCT cells retain a stronger central memory phenotype and exhibit increased persistence. These findings illuminate a unique strategy for engineering therapeutic T cells and improving CAR-T function through synthetic CCT fusion, which is orthogonal to other cell engineering techniques.

Adoptive cellular immunotherapy with engineered CAR-T cells has shown durable clinical responses in hematological malignancies[1]; however, relapse remains a challenge due to factors such as tumor antigen loss, T cell exhaustion, dysfunction and poor in vivo persistence[2,3]. These are among many major challenges with CAR-T therapy, urging for better designs of CARs. Trogocytosis is a process where lymphocytes extract surface molecules from antigen-presenting cells (APCs) through the immune synapse and present them on their own surface[4–6]. This process can lead to the elimination of reactive cytotoxic T lymphocytes through fratricide when large amounts of major histocompatibility complex (MHC)–peptide complexes are acquired and presented[6]. CAR-T cells have been demonstrated to undergo trogocytosis, resulting

[1]Department of Genetics, Yale University School of Medicine, New Haven, CT, USA. [2]System Biology Institute, Yale University, West Haven, CT, USA. [3]Center for Cancer Systems Biology, Yale University, West Haven, CT, USA. [4]Molecular Cell Biology, Genetics, and Development Program, Yale University, New Haven, CT, USA. [5]MD-PhD Program, Yale University, New Haven, CT, USA. [6]Department of Immunobiology, Yale University, New Haven, CT, USA. [7]Yale College, New Haven, CT, USA. [8]Immunobiology Program, Yale University, New Haven, CT, USA. [9]Department of Biomedical Engineering, Yale University, New Haven, CT, USA. [10]Comprehensive Cancer Center, Yale University School of Medicine, New Haven, CT, USA. [11]Stem Cell Center, Yale University School of Medicine, New Haven, CT, USA. [12]Center for Biomedical Data Science, Yale University School of Medicine, New Haven, CT, USA. [13]These authors contributed equally: Xiaoyu Zhou, Hanbing Cao. e-mail: sidi.chen@yale.edu

in tumor antigen loss and fratricide among themselves, compromising their efficacy against cancer[7–9]. Therefore, overcoming CAR-mediated trogocytosis is crucial for durable CAR-T therapeutic effect. Studies suggest that combined targeting of tumor antigens[7] or using low-affinity CAR[8] can rescue CAR-T antitumor responses from trogocytosis-induced immune escape; however, these approaches are not flexible, as they require generating entirely new CARs for each cancer type.

As an immune-checkpoint molecule, cytotoxic T-lymphocyte-associated antigen-4 (CTLA-4) is crucial for maintaining self-tolerance and homeostasis[10]. Initially, CTLA-4 was thought to transmit immune inhibitory signals through its CCT[11]; however, evidence suggests that its inhibitory function is achieved through trans-endocytosis, where CTLA-4$^+$ T cells remove and internalize CD80/CD86 co-stimulatory molecules from APCs, inhibiting CD28 signaling and T cell activation[12–15]. To mediate this process, a key feature of CTLA-4 is that it is highly endocytic and constantly cycling between the cell surface and the intracellular compartment. This cycling occurs through the interaction between the YVKM motif in CCT and clathrin adaptor activating protein 2 (AP-2), resulting in limited surface expression of CTLA-4. Thus, rather than directly transducing suppressive signals, CCT is believed to regulate the surface availability of CTLA-4 for optimal T cell activation[14,16].

In this Article, we utilized CCT to design optimal CAR with low trogocytosis and improved CAR-T therapy efficacy. Fusion of CCTs to CAR's C terminus reduced surface CAR expression through ongoing endocytosis, recycling and degradation. CAR-CCT cells had reduced trogocytosis, reduced activation and production of proinflammatory cytokines. Additionally, CAR-T cells with monomeric (CAR-1CCT) or duplex CCTs (CAR-2CCT) exhibit durable antitumor efficacy in vivo. CAR-2CCT cells exhibit increased persistence and central memory differentiation. Together, these data illuminate a distinct approach to engineer CAR-T cells via synthetic CCT fusions.

Results

CAR with CCT fusion confers CAR-T cell durability

To test whether CCT engineering can improve the functionality of CAR-T cells, we designed lentiviral constructs to express a CD22-CAR (hereafter abbreviated CAR) with monomeric (CAR-1CCT), duplex (CAR-2CCT) or triplex CCTs (CAR-3CCT) fused to the C terminus of CAR (Extended Data Fig. 1a). Transduction of human CD3 T cells with those constructs did not affect the CD4/CD8 T cell composition (Extended Data Fig. 1b,c). We assessed the effector function of the engineered CAR-CCT cells by co-culturing them with NALM6 cells expressing green fluorescent protein (GFP)-luciferase (NALM6GL) (Extended Data Fig. 1d). All CAR-T cells lysed approximately 100% of NALM6GL when co-cultured with one round of cancer cells for 24 h (Extended Data Fig. 1e); however, CAR-T cells with CCT fusions showed significantly higher survival rates. (Extended Data Fig. 1f). CAR-2CCT and CAR-3CCT cells exhibited lower expression of exhaustion markers (LAG3 and PD-1) compared to control CAR-T cells (Extended Data Fig. 1g–j). Other co-inhibitory markers such as TIGIT, cycling CTLA-4 and recycling CTLA-4 were comparable between groups, whereas TIM3 was undetectable in all groups (Extended Data Fig. 1k–p).

We then hypothesized that CAR engineered with CCT fusion might support the persistent T cell response under repeated stimulation, which is commonly seen in cancer relapses. To test this, we introduced a second round of NALM6GL (Extended Data Fig. 1a). CAR-CCT cells showed significantly fewer live NALM6GL cells (Fig. 1a,b and Extended Data Fig. 2a), indicating their superior capability. Moreover, CAR-CCT cells exhibited increased survival after the second round of stimulation (Fig. 1c,d), despite the same number of input CAR-T cells seeded at the beginning of the co-culture (Extended Data Fig. 2b). Notably, CAR-2CCT and CAR-3CCT cells showed higher expression of central memory markers such as CD45RO and CD62L (Extended Data Fig. 2c,d), while maintaining lower LAG3 expression (Extended Data Fig. 2e,f).

To investigate the impact of tumor antigen density on CAR-CCT cells, we co-cultured CAR-CCT cells with either CD22^{high} or CD22^{low} NALM6 cells. We found that CAR-CCT cells induced more efficient killing than the control CAR-T cells, with CAR-2CCT and CAR-3CCT showing the highest capability of killing both CD22^{high} and CD22^{low} NALM6 cells (Extended Data Fig. 2g–i). All four groups of CAR-T cells were more effective at killing cancer cells with lower CD22 expression (Extended Data Fig. 2g–i), indicating that a high cancer antigen load is unfavorable for CAR-T function under repeated challenge in vitro. Altogether, these results suggest that CAR-T cells with engineered CCT fusion have improved durability under repeated antigen stimulations, with enhanced cytolytic ability and a stronger central memory phenotype.

To confirm the versatility of our approach, we similarly engineered a series of CAR and CAR-CCT constructs with a human CD19 targeting CAR (19CAR) (Extended Data Fig. 3a). We noted significantly more 19CAR-T cells survived the two rounds NALM6GL co-culture, which progressively killed more NALM6GL cells with increasing number of CCTs (Extended Data Fig. 3b–d). Collectively, these results demonstrated that harnessing CCT fusion to enhance CAR-T function is applicable to CAR with different specificities.

CAR-CCT cells show reduced activation and cytokine production

We further investigated whether CCT fusion altered CAR signaling and observed that CAR-CCT cells were responsive to antigen stimulation. Increasing CCT fusion decreased the expression level of phospho-ERK1/2 (pT202/pY204), interferon (IFN)-γ and tumor necrosis factor (TNF)-α (Fig. 1e–i). Moreover, CCT-engineered CAR-T cells, especially CAR-3CCT cells, had elevated levels of granzymes, perforin and granulysin, which are the main factors for targeted killing by CAR-T cells[17]. In contrast, CAR-CCT cells had reduced levels of proinflammatory cytokines, such as IL-4, IL-6, IL-2, TNF-α, IL17a and IFN-γ (Extended Data Fig. 3e), all of which are associated with cytokine release syndrome (CRS) seen in clinical CAR-T therapy[18,19]. These data suggest that engineered CAR-CCT cells have improved killing capability with elevated degranulation, but decreased ERK phosphorylation, IFN-γ and TNF-α production. Given the increased in vitro killing ability and elevated granzymes, CAR-CCT cells are more efficient in their ability to kill cancer cells.

Fig. 1 | Engineering CAR with CCT fusion increased persistent CAR-T cell function under repeated tumor stimulation. a, Quantification of NALM6GL percentage after two rounds of NALM6GL stimulation, $n = 6$. **b**, Quantification of NALM6GL counts after two rounds of NALM6GL stimulation, $n = 6$. **c**, Quantification of CAR-T cell percentage after two rounds of NALM6GL stimulation, $n = 3$. **d**. Quantification of CAR-T cell counts after two rounds of NALM6GL stimulation, $n = 3$. **e**, Representative FACS plots demonstrating the expression of pERK1/2(pT202/pY204) after crosslinking CAR-T cells with CD22-biotin and streptavidin at 37 °C for 5 min. All CAR-T cells were previously gated on mScarlet$^+$ populations for quantification. **f**, Quantification of pERK1/2(pT202/pY204) expression in CAR-T cells as shown in **e**, $n = 3$. **g**, Representative FACS plots demonstrating the intracellular expression of IFN-γ and TNF-α by CAR-T cells after stimulated with NALM6GL cells at an E:T (effector:target) ratio of 1:1 for 4 h. **h**,**i**, Quantification of intracellular IFN-γ (**h**, $n = 3$) and TNF-α (**i**, $n = 6$) expression as shown in **g**. For all bar plots, data are shown as mean ± s.e.m. One-way analysis of variance (ANOVA) with Dunnett's multiple-comparisons test was used to assess significance (**h**,**i**). Two-way ANOVA with Tukey's multiple-comparisons test is used to assess significance (**a**–**d**). Exact *P* values are labeled above all comparisons. All numbers defined by '*n*' indicate the number of biologically independent samples. Data are representative of three independent experiments.

https://doi.org/10.1038/s41590-023-01571-5

The accompanying decrease in ERK phosphorylation, IFN-γ and TNF-α production may imply a reduction in T cell activation and inflammatory responses, possibly due to alterations in CAR dynamics after CCT fusion. The phenomenon that engineered T cells with enhanced cytotoxicity, but low cytokine release, has also been reported by others[20,21], potentially limiting the risk of CRS and cerebral edema/neurotoxicity, two major side effects associated with current CAR-T cell therapy[22].

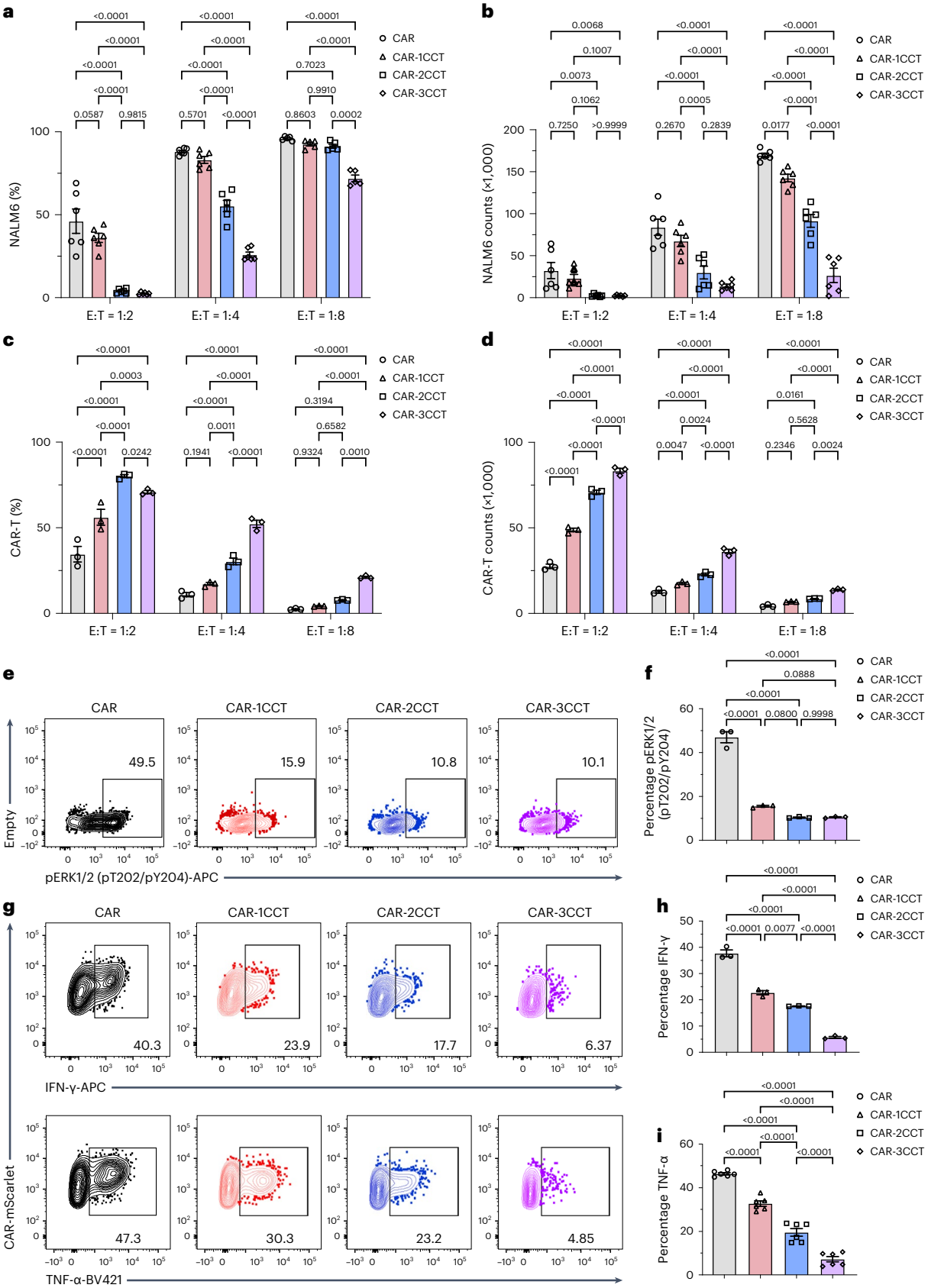

https://doi.org/10.1038/s41590-023-01571-5

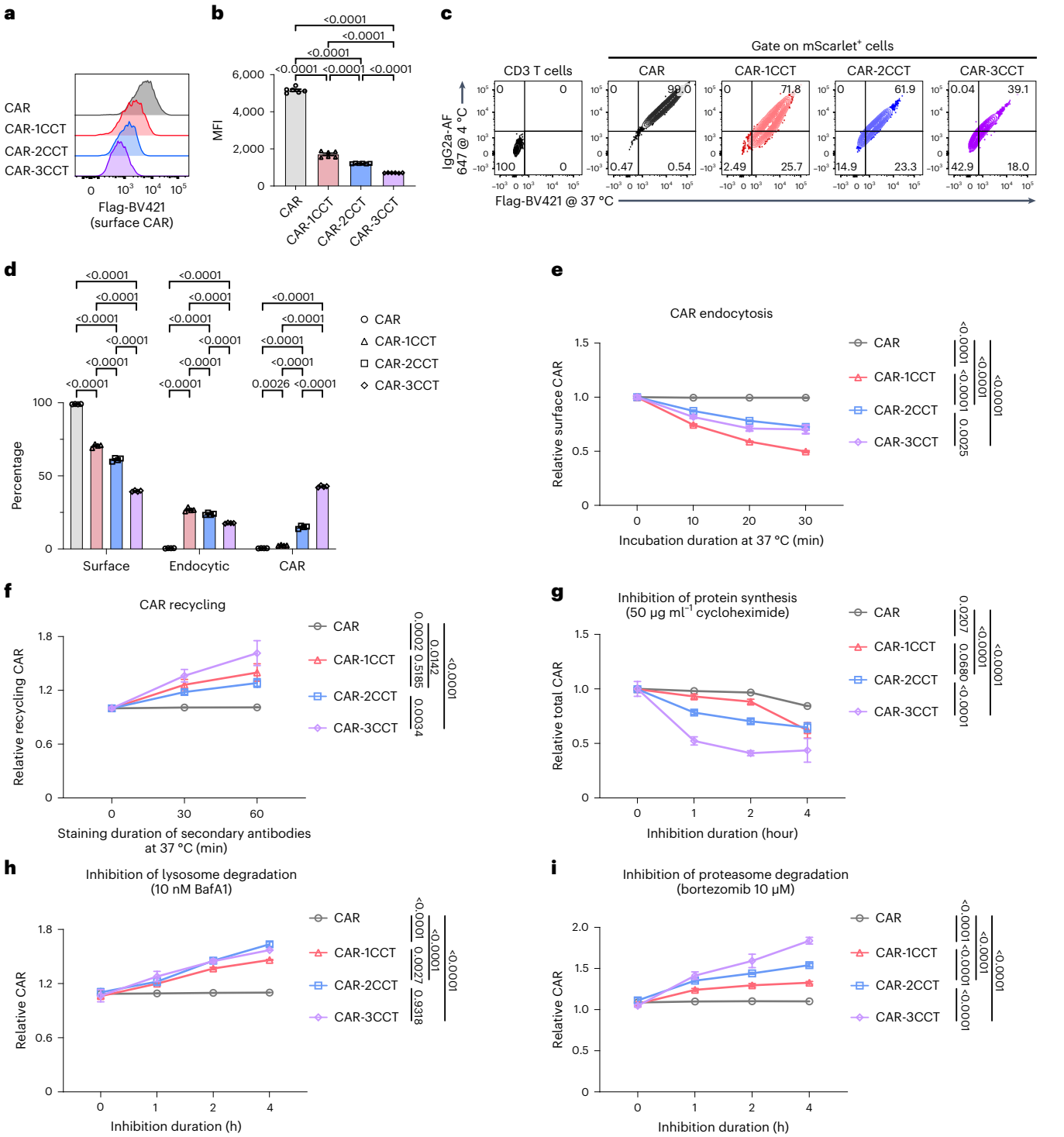

Fig. 2 | CCT fusion enables titration of CAR expression through receptor endocytosis, recycling and degradation at steady state. a, Representative flow cytometry analysis of CAR-T cells, pre-gated on mScarlet$^+$ populations, showing surface expression level of CAR, indicated by Flag staining. **b**, Quantification of **a** showing surface Flag expression on CAR-T cells in median fluorescence intensity (MFI), $n = 6$. **c**, Representative flow cytometry analysis of CAR-T endocytosis, see Extended Data Fig. 4a for detailed workflow. **d**, Quantification of **c** showing the level of CAR-T endocytosis, $n = 4$. **e**, Quantification of endocytosis CAR over time, see Extended Data Fig. 4b for detailed workflow, $n = 3$. **f**, Quantification of recycling CAR over time, see Extended Data Fig. 4c for detailed workflow, $n = 6$. **g**, Quantification of the stability CAR with the presence of 50 μg ml^{-1} cycloheximide by intracellular staining of Flag. Relative CAR expression was determined by dividing the proportion of Flag$^+$ CAR-T cells after treatment using cycloheximide with those treated using DMSO (0 h), $n = 3$. **h**,**i**, Quantification of CAR expression in the presence of 10 nM BafA1 (**h**, $n = 3$) or 10 μM bortezomib (**i**, $n = 3$) by performing intracellular staining of CAR-T cells that had been previously fed with anti-Flag antibody at 37 °C for 1 h, followed by detection using anti-rat-IgG2a-AlexaFluor 647 specific to the primary antibody. Relative CAR expression was determined by dividing the proportion of Alexa Fluor 647$^+$ CAR-T cells after treatment using degradation inhibitors with those treated using DMSO (0 h). For all bar plots, data are shown as mean ± s.e.m. One-way ANOVA with Dunnett's multiple-comparisons test is used to assess significance for **b**. Two-way ANOVA with Tukey's multiple-comparisons test is used to assess significance for **d**–**i**. Exact *P* values are labeled above all comparisons. All numbers defined by 'n' indicate the number of biologically independent samples. Data are representative of two independent experiments.

https://doi.org/10.1038/s41590-023-01571-5

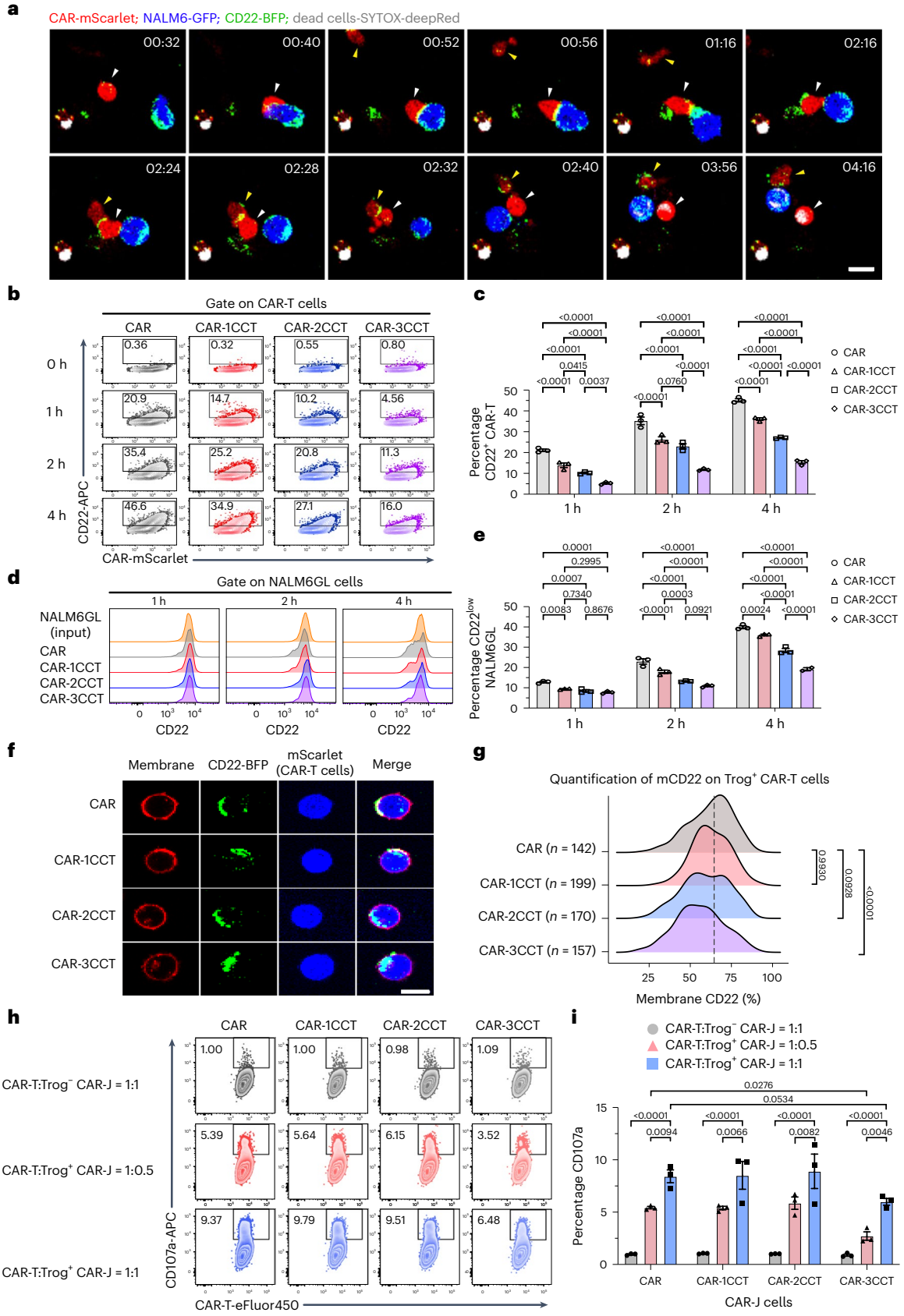

CCT fusion alters CAR endocytosis, recycling and degradation

CTLA-4 is constantly internalized through endocytosis, with subsequent recycling or degradation[23–25]. To gain insight into the improved killing ability and reduced activation of CAR-CCT cells, we investigated if CARs with CCT fusion also possess similar molecular dynamics as native CTLA-4. We observed that CCT fusion reduced surface CAR expression in a dose-dependent manner (Fig. 2a,b). And this decreased surface CAR expression and may explain the decreased activation

Fig. 3 | CCT fusion effectively decreases CAR-mediated trogocytosis and accompanying fratricide. a, Representative timelapse live cell images showing trogocytosis and fratricide of CAR-T cells. The white arrow labels a CAR-T cell that acquired CD22-BFP, which subsequently rendered it susceptible to CAR-T fratricide, as indicated by the influx of SYTOX deep red dye. This white arrow-labeled cell then contacted with another CAR-T cell (yellow arrow), interacting at a region with enhanced CD22-BFP signal. Shortly after this active interaction, the white arrow-labeled cell was stained by the SYTOX deep red dye, indicating cell death. The time stamps on the top right of each image are represented as hour:minute. Scale bar, 10 µm. **b**, Representative flow cytometry results showing CD22 expression on CAR-T cells after 0–4 h co-culturing with NALM6GL cells at E:T ratio of 1:1. **c**, Quantification of **b** showing CD22 expression on CAR-T cells, $n = 3$. **d**, Representative flow cytometry results showing CD22 expression on NALM6GL cells after 0–4 h co-culturing with CAR-T cells at E:T ratio of 1:1. **e**, Quantification of **d** showing CD22 expression on NALM6GL cells, $n = 3$. **f**, Representative confocal images showing the CD22-BFP colocalization with surface membrane of Trog$^+$ CAR-T cells. Scale bar, 10 µm. **g**, Quantification of **f** showing the distribution of % membrane CD22 (mCD22). In each group, the total number of quantified cells is labeled on the *y* axis of the plot. The dashed line represents the median percentage of mCD22 on the control CAR-T cells. **h**, Representative flow cytometry results showing the CD107a expression of fresh CAR-T cells in co-culture with Trog$^+$ or Trog$^-$ CAR-J cells at various E:T ratios (see Extended Data Fig. 5e for detailed workflow). **j**, Quantification of **i**, $n = 3$. For all bar plots, data are shown as mean ± s.e.m. One-way ANOVA with Dunnett's multiple-comparisons test was used to assess significance (**g**). Two-way ANOVA with Tukey's multiple-comparisons test was used to assess significance (**c**,**e**,**i**). Exact *P* values are labeled above all comparisons. All numbers defined by '*n*' indicate the number of biologically independent samples. Data are representative of two independent experiments.

level seen in CAR-CCT cells following antigen stimulation (Fig. 1e–i). Moreover, when comparing the CCT fusion with encoding CAR using a weaker promoter that has only minimal cytomegalovirus (CMV) promoter sequences without any enhancer element (mCMV-CAR)[26], CAR-CCT cells exhibited significantly lower surface CAR expression (Extended Data Fig. 3f–h). Additionally, we noted that CARs with CCT fusion had altered cellular localization patterns and displayed endocytic features, with CAR-1CCT displaying the highest endocytosis level (Fig. 2c,d and Extended Data Fig. 4a). We again observed that with increasing CCT fusion, surface CAR levels decreased. CAR-3CCT cells had the highest number of mScarlet$^+$CAR$^-$ populations (Fig. 2c,d), suggestive of elevated degradation of CAR-3CCT molecules. Furthermore, CAR-1CCT was noted to display the highest endocytosis rate (Fig. 2e and Extended Data Fig. 4b), consisting with its highest endocytosis level shown in Fig. 2d. Moreover, we found that in contrast to the control CAR, CAR-CCT molecules showed recycling features, with CAR-3CCT showing the highest recycling rate, and CAR-1CCT and CAR-2CCT demonstrating similar recycling rates (Fig. 2f and Extended Data Fig. 4c).

We additionally quantified the stability of the CAR-CCT molecules at steady state. By inhibiting de novo protein translation with cycloheximide[27], we observed significantly decreased stability of CAR-CCT molecules, with CAR-3CCT molecules demonstrating the highest degradation rate (Fig. 2g). We then assessed the degradation pathway by introducing inhibitors for lysosomal (bafilomycin A1; BafA1) and proteasomal (bortezomib) degradation. Treatment with BafA1 or bortezomib increased relative CAR expression in CAR-CCT groups, suggesting that both the lysosome and proteasome are involved in CAR-CCT degradation (Fig. 2h,i). Increasing the number of CCT fusions in CAR-CCT cells led to a dose-dependent increase in proteasomal degradation when treated with bortezomib (Fig. 2i). Inhibition of lysosomal degradation by BafA1 showed no difference in CAR expression between CAR-3CCT and CAR-2CCT, although both had increased lysosomal degradation compared to 1CCT and baseline CAR (Fig. 2h). These findings indicate that CCT fusions promote lysosomal degradation up to a certain point (2CCT), while increasing CCT fusions progressively promote proteasomal degradation up to 3CCT. Notably, CAR-1CCT displayed the highest endocytosis, whereas 3CCT exhibits the highest degradation, implying that increased CCT fusions make CAR molecules more susceptible to degradation. Collectively, these data suggest that the expression of CAR-CCT molecules is regulated by their constant endocytosis, recycling and degradation, contrasting with that of the control.

CCT fusion reduces CAR-mediated trogocytosis

CAR-T cells can acquire surface molecules from tumor cells through trogocytosis, leading to antigen loss that compromises antitumor efficacy[7]. To investigate this, we performed timelapse live cell imaging and found that CAR-T cells actively acquired CD22 antigen from NALM6GL cells (Supplementary Video 1). Fratricide among CAR-T cells was also recorded, indicated by the influx of a dye after active engagement between CD22$^+$ CAR-T cells (Fig. 3a and Supplementary Video 1). Moreover, we found that latrunculin A, an F-actin inhibitor[7,28], inhibits the transfer of CD22 antigen from NALM6 cells to T cells, a hallmark of CAR-mediated trogocytosis (Extended Data Fig. 5a,b), which further supports the observations.

As trogocytosis can be impacted by CAR affinity[29], we wondered whether the altered molecular dynamics of CAR-CCT might also impact CAR-mediated trogocytosis. We detected substantial surface CD22 antigen on CAR-T cells that normally do not express CD22 as early as 1 h after incubation, indicating rapid trogocytosis by CAR-T cells (Fig. 3b,c). CCT fusion significantly reduced trogocytosis-mediated acquisition of surface CD22 in a CCT-dose-dependent fashion (Fig. 3b,c and Extended Data Fig. 5a,b). Concordantly, NALM6GL cancer cells retained progressively more surface CD22 antigen when co-cultured with CAR-T cells harboring increasing numbers of engineered CCTs (Fig. 3d,e). These results showed that CCT fusion efficiently reduces CAR-mediated trogocytosis and CD22 loss in cancer cells.

Fig. 4 | CAR-T cells with CCT fusion show increased survival and proliferation. **a**, Representative flow cytometry results showing the relative survival of 19CAR-T cells from the assay described above (see Extended Data Fig. 5f for detailed workflow). **b**, Quantification of **a** showing the relative survival of 19CAR-T cells ($n = 3$) and 19CAR-CCT cells ($n = 6$). **c**, Quantification of relative survival of CAR-T cells (CD22-CAR-T) using the assay described in Extended Data Fig. 5f, $n = 3$. **d**, Representative flow cytometry results showing the dilution of proliferation staining dye (eFluor450). Purified CAR-T cells were stained with 10 µM eFluor450 and cultured in cX-vivo medium for 4 d before being analyzed by flow cytometry. The number labeled on the plot indicates the division number modulated using FlowJo. **e**, Quantification of **d** showing the percentage of proliferated CAR-T cells corresponding to each division number, $n = 4$. **f**. Representative flow cytometry results showing the Live/Dead and annexin V staining of sorted Trog$^+$ and Trog$^-$ CAR-T cells (see Extended Data Fig. 5g for detailed workflow). **g**, Quantification of **f** showing the percentage of annexin V$^+$ CAR-T cells, $n = 3$. **h**, Representative flow cytometry results showing in vivo relative survival of CAR-T cells using the assay described in Extended Data Fig. 6d. **i**, Quantification of **h** showing the relative survival of CAR-T cells, $n = 4$. **j**, Quantification of CAR-T trogocytosis in vivo as indicated by the CD22 expression detected by staining CAR-T cells from above BM, $n = 4$. **k**, Correlation between relative survival and trogocytosis of CAR-T cells, $n = 4$. **l**, Quantification of CAR-T cell and NALM6GL relative abundance by calculating the CAR-T:NALM6GL ratio, $n = 4$. For all bar plots, data are shown as mean ± s.e.m. One-way ANOVA with Dunnett's multiple-comparisons test was used to assess significance (**b**,**c**,**i**,**j**,**l**). Two-way ANOVA with Tukey's multiple-comparisons test was used to assess significance (**e**,**g**). Simple linear regression was used to fit data shown in **k**. Exact *P* values are labeled. All numbers defined by '*n*' indicate the number of biologically independent samples. Data are representative of two independent experiments.

https://doi.org/10.1038/s41590-023-01571-5

As CTLA-4 has been shown to internalize ligands acquired by trans-endocytosis[13], we quantified the localization of the transferred CD22 antigen, and noted that majority of the transferred CD22 antigen localized to the cell membrane (Fig. 3f,g). Only 3CCT fusion seemed to decrease membrane colocalization, given that a significant leftward shift of the membrane CD22(%) distribution was only observed for CAR-3CCT (Fig. 3g). Thus, the presence of 1CCT or 2CCT fusion does not significantly change the surface localization of CD22

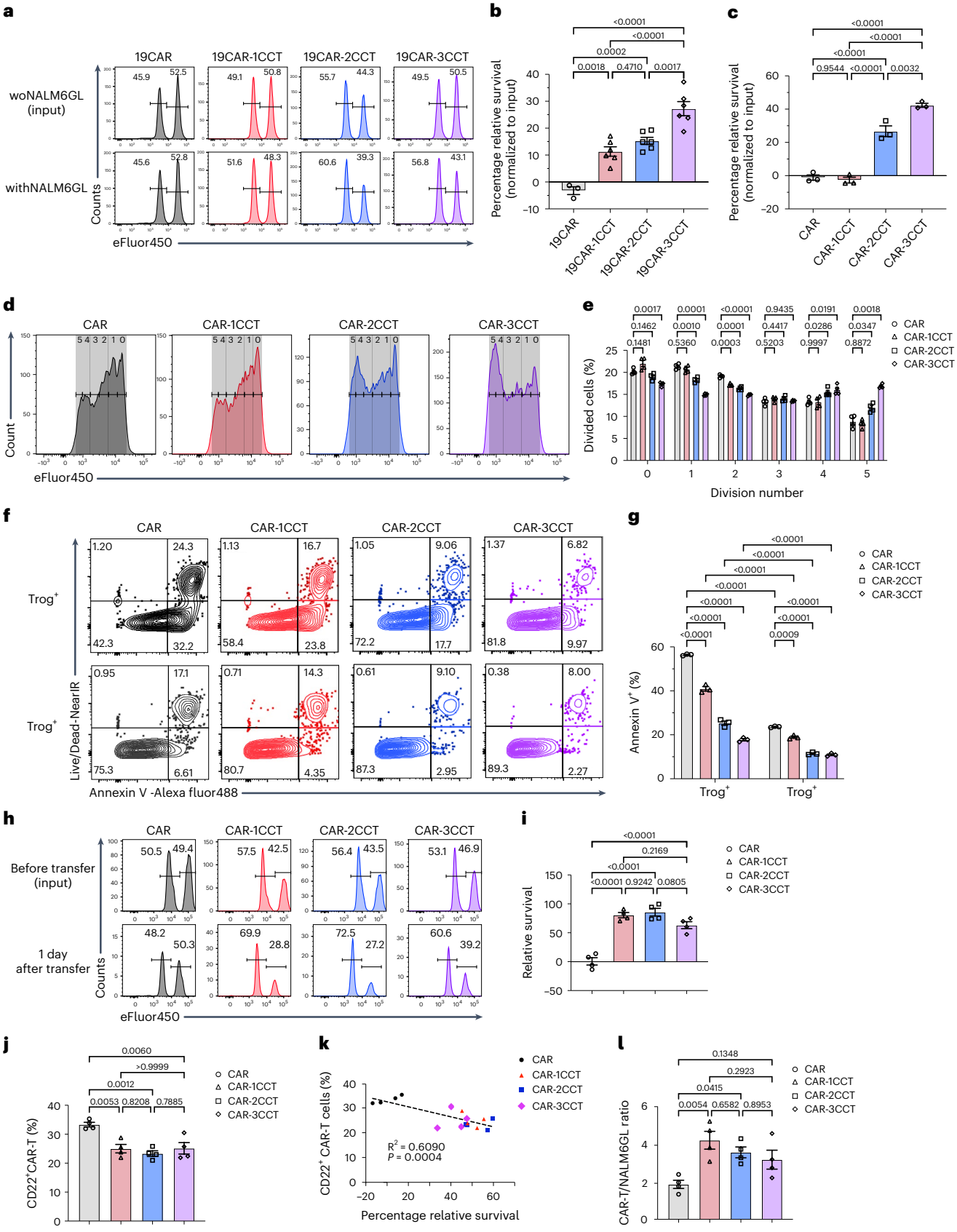

molecules obtained through trogocytosis, whereas 3CCT fusion leads to increased internalization.

To determine whether the CD22 antigen acquired by trogocytosis is still functional, we generated CAR-Jurkat (CAR-J) cells, which undergo trogocytosis of target CD22 (Extended Data Fig. 5c,d) without killing the target cells[30]. We noted that in all groups, CD22-GFP$^+$ (Trog$^+$) CAR-J cells could induce the cytotoxic degranulation of CAR-T cells, as indicated by the membrane expression of CD107a. This was achieved in a dose-dependent manner, as higher degranulation occurred when more target Trog$^+$ CAR-J cells were added to the co-culture (Fig. 3h,i and Extended Data Fig. 5e). Given that significantly lower percentages of Trog$^+$ were observed in the CAR-CCT cells after their encounter with cancer cells (Fig. 3b,c), lower degranulation and thus lower fratricide among them could be inferred. In comparison, CD22-GFP$^-$ (Trog$^-$) CAR-J cells did not meaningfully induce degranulation, as expected (Fig. 3i). These data indicate that CD22 transferred through trogocytosis is functional in stimulating CAR-T cell degranulation. While the stimulation of CAR-T degranulation was similar among Trog$^+$ control CAR-J cells, CAR-1CCT-J and CAR-2CCT-J cells, Trog$^+$ CAR-J cells with 3CCT fusion induced significantly lower degranulation (Fig. 3h,i). This may result from the enhanced internalization of transferred CD22 by CAR-3CCT, as seen in Fig. 3g. Together, these results suggest that CCT fusion quantitively reduces CAR-mediated trogocytosis, loss of cancer antigen.

CCT fusion enhances CAR-T cell survival and proliferation

Given our observation that CAR-CCT cells were more abundant after repeated stimulation and exhibited reduced trogocytosis, we investigated the impact of CCT fusion on CAR-T cell survival and proliferation and noted that CAR-T cells with CCT fusion exhibited improved survival than the control (Fig. 4a–c and Extended Data Fig. 5f). A proliferation assay revealed that CAR-2CCT and CAR-3CCT cells exhibited greater proliferation potential, as more cells underwent four or five rounds of division (Fig. 4d,e). In addition, we observed that Trog$^+$ CAR-T cells were significantly more apoptotic than the Trog$^-$ CAR-T cells and that CAR-T cells with increasing CCT fusion had reduced apoptosis levels (Fig. 4f,g and Extended Data Fig. 5g). Furthermore, we observed minimal expression of Fas or FasL, with all groups showing similar levels of Fas/FasL, though there was a slight decrease in the expression of FasL on CAR-CCT cells 4 h after stimulation (Extended Data Fig. 6a–c). This suggests that the significantly improved survival of CAR-CCT cells is unlikely to be attributed to Fas/FasL-mediated activation induced cell death (AICD)[31]. Collectively, these results suggest that the high levels of trogocytosis induced by the control CAR are unfavorable for T cell survival and that CAR-CCT fusion inhibits this process to improve CAR-T survival following antigen exposure.

We next investigated whether the enhanced survival of CAR-CCT cells was also evident in vivo. We collected adoptively transferred CAR-T cells from bone marrow (BM), where most cancer cells reside[32], and found that CAR-CCT cells showed significantly higher relative survival (Fig. 4h,i and Extended Data Fig. 6d,e) and lower trogocytosis levels (Fig. 4j). Notably, we observed a strong correlation between the relative survival and trogocytosis of the CAR-T cells (Fig. 4k), with higher survival corresponding to lower trogocytosis. This was consistent with results showing higher CAR-T:NALM6GL ratios in CAR-1CCT or CAR-2CCT cells (Fig. 4l). These findings collectively demonstrate that CCT fusion effectively improves the survival and proliferation of CAR-T and impairs the high level of apoptosis associated with trogocytosis.

CAR-T cells with CCT fusion show distinct transcriptomes

To understand the impact of CCT fusion engineering on CAR-T cells, we conducted messenger RNA sequencing on them, both at baseline and after two rounds of NALM6GL stimulation. Principal-component analysis (PCA) showed distinct group separation among different CAR-T groups (Supplementary Table 1 and Extended Data Fig. 7a–c). At baseline without NALM6GL stimulation, CAR-CCT cells displayed reduced tonic signaling, as indicated by lower expression of inhibitory receptors (Extended Data Fig. 7d). High expression of these genes without antigen stimulation is consistent with antigen-independent activation of CARs, a hallmark of tonic signaling that can result in exhaustion[33,34]. Flow cytometry analysis of LAG3, HHLA2 and CD101 confirmed these findings at the protein level (Extended Data Fig. 7e–g). Of note, RNA-seq analysis of CAR-T cells undergoing repeated cancer stimulations revealed a notable impact of synthetic CCT fusion on the transcriptome. With increasing numbers of fused CCTs, more differentially expressed genes (DEGs) were identified (Supplementary Table 1 and Extended Data Fig. 7h). Pathway analysis revealed many enriched differentially altered pathways. CAR-2CCT cells upregulated genes that are enriched in cell chemotaxis, leukocyte migration and regulation of cytosolic calcium ion concentration, indicating enhanced responsiveness of CAR-T cells to repeated stimulations (Supplementary Table 1 and Extended Data Fig. 7i). Among commonly upregulated genes, *GZMK, CD244, CCR2, CCR5, CXCR6* and *KLF2* are related to effector T functions, which were significantly upregulated CAR-CCT cells. Notably, we observed 20 upregulated DEGs unique to CAR-2CCT cells (Extended Data Fig. 7j). Among these, *IL1R1* (ref. 35) and *EPAS1* (ref. 36) can directly enhance the effector function of T cells against tumors. Together, these results demonstrate that CCT fusion can reduce tonic signaling of CARs at baseline, while preserving responsiveness of CAR-T cells to repeated stimulations.

CAR-1CCT or CAR-2CCT cells exhibit superior in vivo efficacy

To assess the in vivo performance of CAR-CCT cells, we established a relapsed leukemia mouse model (Fig. 5a). We detected relapse in mice treated with the control CAR-T as early as day 37, when no obvious signal was detected in mice treated with CAR-1CCT or CAR-2CCT cells (Fig. 5b,c). CAR-1CCT cells efficiently controlled leukemia development in NSG mice, leading to significantly reduced tumor burden and significantly better survival than the control CAR-T cells (Fig. 5c,d). CAR-2CCT cells had remarkably enhanced efficacy, in which all mice

Fig. 5 | CAR-T with 1CCT or 2CCT fusion demonstrated improved antitumor efficacy in a relapsed leukemia mouse model with increased persistence and T_{CM} differentiation. a, Schematics of the in vivo experimental workflow used in **c**,**d**. **b**, Representative bioluminescence imaging of mouse model after CAR-T treatment. For the mock T and CAR-3CCT group, $n = 7$; the remaining groups, $n = 5$. **c**, Quantification of **b** showing the tumor burden as indicated by total radiance (p s^{-1} cm^{-2} sr^{-1}). Two-way ANOVA with Tukey's multiple-comparisons test was used to assess significance. All comparisons with mock T group were conducted with data collected before day 32 (including day 32). *P* values for comparisons are shown below the figure. For the mock T and CAR-3CCT group, $n = 7$; the remaining groups, $n = 5$. **d**, Survival curve of NSG mice in **b**. Mantel–Cox test was used to assess significance. *P* values comparisons are shown below the figure. For the mock T and CAR-3CCT group, $n = 7$; the remaining groups, $n = 5$. **e**, Schematics of the workflow demonstrating the in vivo phenotyping of CAR-T cells. **f**, Representative flow cytometry results showing abundance of CAR-T cells and NALM6GL cells in the spleen (top) and the CD45RO$^+$CD62L$^+$ T_{CM} cells in the BM (bottom). **g**,**h**, Quantification of **f** showing CAR-T counts (**g**, $n = 3$) and the percentage of CD45RO$^+$CD62L$^+$ T_{CM} CAR-T cells (**h**, $n = 3$). **i**, UMAP visualization of CAR-T cells based on their transcriptomes profiled by scRNA-seq. Twelve distinct clusters were identified and annotated. T_{EM}, effector memory T cells; T_{EX}-like, exhausted-like T cells; T_{SCM}, stem memory T cells. **j**, Violin plots showing the expression levels of representative marker genes across 12 clusters. **k**, Relative proportions of each cell type in BM identified by scRNA-seq, across four CAR-T groups. For all bar plots, data are shown as mean ± s.e.m. One-way ANOVA with Dunnett's multiple-comparisons test was used to assess significance (**g**,**h**). Exact *P* values are labeled. All numbers defined by '*n*' indicate the number of biologically independent samples. Data are representative of two independent experiments.

https://doi.org/10.1038/s41590-023-01571-5

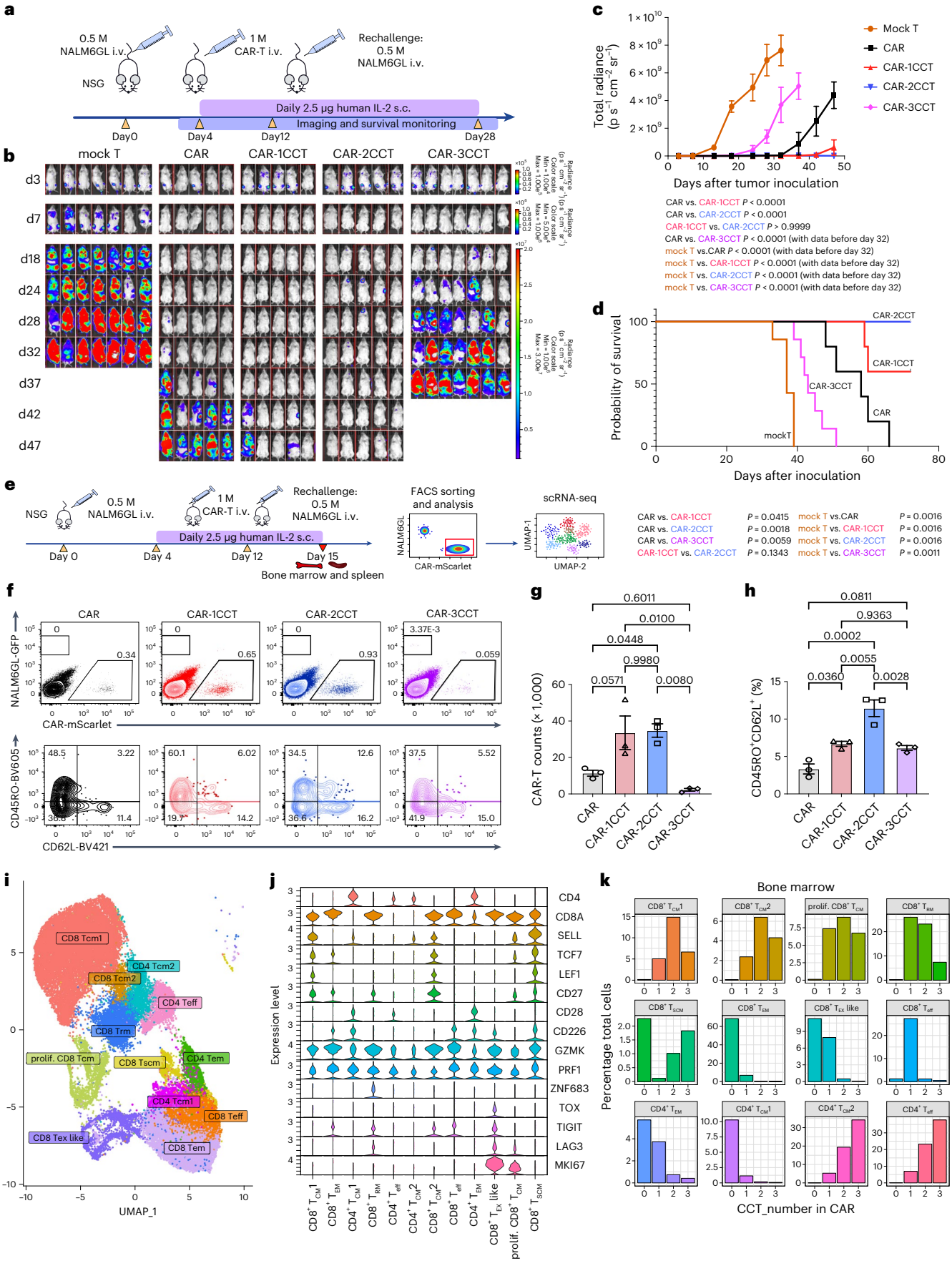

were in full remission against two cancer challenges, with 100% survival and nearly no detectable tumor (Fig. 5b–d). Notably, mice treated with CAR-3CCT cells had earlier relapses than those with CAR-T cells, indicating that triplex CCTs did not improve in vivo CAR-T efficacy over the control CAR-T cells. These data suggest that engineering CAR-T with monomeric or duplex CCTs significantly enhanced in vivo therapeutic efficacy against relapsed leukemia.

2CCT fusion boosts CAR-T cell persistence and central memory

Despite a higher relative survival rate observed in CAR-3CCT cells shortly after their adoptive transfer (Fig. 4h,i), CAR-3CCT cells fail to maintain long-term antitumor efficacy, suggesting that factors other than initial survival contribute to their weakened antitumor effects in vivo. To investigate this, we performed immunological characterization (Fig. 5e), and noted that CAR-1CCT and CAR-2CCT cells showed an upward trend in abundance in the spleen, with CAR-2CCT cells exhibiting a significant increase, whereas CAR-3CCT cells were nearly undetectable. (Fig. 5f,g). CAR-1CCT and CAR-2CCT cells had a notably higher fraction of central memory T (T_{CM}) cells ($CD45RO^+$;$CD62L^+$), with CAR-2CCT cells having the highest T_{CM}% level; in contrast, CAR-3CCT cells did not have an increase in T_{CM} cells (Fig. 5f,h). These data showed that CAR-T engineering with 1CCT and particularly 2CCT, but not 3CCT, enhanced in vivo persistence and T_{CM} development, consistent with their superior efficacy in vivo.

We additionally used single-cell RNA-seq (scRNA-seq) to characterize the full spectrum of engineered CAR-T cells and their transcriptomic profiles (Fig. 5e). We mapped the transcriptomes of 39,151 single CAR-T cells via Uniform Manifold Approximation and Projection (UMAP) and identified 12 distinct clusters (Fig. 5i, Extended Data Fig. 8a and Supplementary Table 2). We annotated those clusters based on their expression profile of known immune-cell markers (Fig. 5j, Extended Data Fig. 8b and Supplementary Table 2). Samples isolated from BM consisted of a higher level of heterogeneity than those from spleen, as more diverse T cell states were identified in CAR-T populations from BM (Extended Data Fig. 8c).

scRNA-seq of the CAR-CCT cells revealed substantial changes in cell subset composition compared to the control in the BM but not spleen (Extended Data Fig. 8d,e). We observed an increase of $CD8^+$ $T_{CM}1$, $CD8^+$ $T_{CM}2$, proliferating (prolif.) $CD8^+$ T_{CM} and $CD8^+$ tissue-resident T ($CD8^+$ T_{RM}) cells in CAR-1CCT and CAR-2CCT particularly (Fig. 5k). We again observed major differences in T_{CM} populations. CAR-2CCT cells from BM had the highest proportion of $CD8^+$ T_{CM} cells among all groups (Fig. 5k and Extended Data Fig. 8d). We further analyzed DEGs between CAR-2CCT and CAR-3CCT, which had the most distinct in vivo efficacy. In most T cell clusters, the number of DEGs are small (Supplementary Table 2). We noticed that within $CD4^+$ effector T (T_{eff}) cell cluster in BM, effector markers such as *KLRB1*, *KLRK1*, *KLRG1*, *NKG7*, *GZMK* and *CTSW* were significantly upregulated in the CAR-2CCT compared to the CAR-3CCT group (Extended Data Fig. 8f). This suggests that $CD4^+$ T_{eff} cells from the CAR-2CCT group have a more activated and cytotoxic phenotype compared to those from the CAR-3CCT group. Taken together, these data suggest that the improved in vivo efficacy achieved by CAR-1CCT and CAR-2CCT cells is linked to their enhanced persistence and T_{CM} cell development in vivo.

Discussion

Cell-based therapeutics have demonstrated great promise; however, durable remissions are only observed in a limited number of patients[37]. Improving the clinical efficacy of CAR-T cell therapy thus necessitates the development of new strategies to prevent relapse. By harnessing the unique dynamic features of CCT and fusing it to C-terminal CAR, we altered the dynamics of CAR molecules by accelerating their endocytosis, degradation and recycling. This in turn led to reduced T cell activation, inflammatory cytokine production, limited trogocytosis and cancer antigen loss, ameliorating the potential for subsequent CAR-T fratricide. Moreover, CAR-1CCT and CAR-2CCT cells showed improved survival and persistence and T_{CM} development in vivo, with enhanced anticancer functionality (Extended Data Fig. 9).

Trogocytosis is well-documented process that mediates surface molecule transfer from target cells to immune populations such as T[6], B[4] and natural killer (NK)[5] cells. CAR-mediated trogocytosis can impair efficacy of both CAR-NK[38] and CAR-T[7,8] cell-based therapies; however, existing strategies reducing CAR-mediated trogocytosis are limited. The CCT fusion approach introduces a new molecular feature to CARs, allowing dynamic control of surface CAR expression at the protein level and effectively reducing trogocytosis. We demonstrated quantitative regulation of CAR-mediated trogocytosis by adjusting the number of CCT fusions. Our study therefore builds on previous work regarding the impact of target antigen density[39] and the affinity of CAR[8] on trogocytosis. Our study is the first to show that CAR-mediated trogocytosis can be quantitatively regulated by adjusting the number of CCT fusions. This approach involves engineering the distal cytoplasmic end of the CAR, which can apply to receptors with different antigen specificities. We show here that the properties of CCT fusion are also applicable to CD19-specific CARs, indicating its versatility. In the future, CCT fusion might also be tested to control trogocytosis mediated by other cellular therapies such as CAR-NK cells, as NK cells have similar CTLA-4 endocytosis[40,41]. Besides the regulation of trogocytosis, CCT fusion effectively improved CAR-T survival in vitro and in vivo, while also leading to reduced apoptosis. These observed phenomena were partially due to decrease in trogocytosis and fratricide among CAR-CCT cells; however, their increased proliferation and altered differentiation also play important roles.

The interaction strength between CAR and its cognate antigen is crucial for CAR-T function[42]. Regulating CAR signaling strength with CCT fusion prevents CAR-T cells from excessive stimulation and enables durable response against tumor cells. It is essential to tightly regulate CAR signaling to achieve a balanced level of signaling for effective tumor antigen detection and CAR-T action, while avoiding detrimental effects associated with high affinity or expression[43–45]. This resonates in our results that CAR-3CCT cells had the best killing capability in vitro but performed worse than control CAR-T cells in vivo. This suggests that optimal CAR signaling strength differs between in vitro and in vivo. In vitro assays benefit from reduced CAR surface expression, allowing sufficient tumor cell killing while minimizing exhaustion and fratricide; however, in the in vivo setting, diluted CAR-T cells require higher CAR signaling strength to overcome lower cell density. CAR-2CCT cells may land in a local optimum for in vivo efficacy with balanced cellular features. Generally, our study highlights the importance of in vivo studies to titrate CAR signaling strength, as in vitro co-culture assays often cannot recapitulate such complexities.

Other studies have proposed approaches to modulate CAR signaling strength, such as transient cessation of CAR signaling with a multi-kinase inhibitor[46], lower affinity CARs[44] and regulated promoters[47,48]. CCT fusion offers distinct advantages over these approaches as it allows for tunable regulation of CAR surface availability without additional chemicals or engineering new CARs. This simplicity is advantageous compared to regulated promoters, which require extensive tailoring and redesigning. Furthermore, CCT fusion regulates CAR availability at protein level, offering potential for self-regulation by introducing a protease module. This enables control over the timing and duration of CAR expression, optimizing efficacy with limited toxicity. Overall, we demonstrate that fine-tuning CAR dynamics with CCT fusion can improve the antitumor efficacy of CAR-T cell therapy, illuminating an orthogonal strategy to develop more effective CAR-T cell therapies.

Online content

Any methods, additional references, Nature Portfolio reporting summaries, source data, extended data, supplementary information,

acknowledgements, peer review information; details of author contributions and competing interests; and statements of data and code availability are available at https://doi.org/10.1038/s41590-023-01571-5.

References

1. June, C. H. & Sadelain, M. Chimeric antigen receptor therapy. *N. Engl. J. Med* **379**, 64–73 (2018).
2. Orlando, E. J. et al. Genetic mechanisms of target antigen loss in CAR19 therapy of acute lymphoblastic leukemia. *Nat. Med* **24**, 1504–1506 (2018).
3. Majzner, R. G. & Mackall, C. L. Tumor antigen escape from CAR T-cell therapy. *Cancer Discov.* **8**, 1219–1226 (2018).
4. Schriek, P. et al. Marginal zone B cells acquire dendritic cell functions by trogocytosis. *Science* **375**, eabf7470 (2022).
5. Lu, T. et al. Hijacking TYRO3 from tumor cells via trogocytosis enhances NK-cell effector functions and proliferation. *Cancer Immunol. Res.* **9**, 1229–1241 (2021).
6. Huang, J. F. et al. TCR-Mediated internalization of peptide-MHC complexes acquired by T cells. *Science* **286**, 952–954 (1999).
7. Hamieh, M. et al. CAR T cell trogocytosis and cooperative killing regulate tumour antigen escape. *Nature* **568**, 112–116 (2019).
8. Olson, M. L. et al. Low-affinity CAR T cells exhibit reduced trogocytosis, preventing rapid antigen loss, and increasing CAR T cell expansion. *Leukemia* **36**, 1943–1946 (2022).
9. Rurik, J. G. et al. CAR T cells produced in vivo to treat cardiac injury. *Science* **375**, 91–96 (2022).
10. Tivol, E. A. et al. Loss of CTLA-4 leads to massive lymphoproliferation and fatal multiorgan tissue destruction, revealing a critical negative regulatory role of CTLA-4. *Immunity* **3**, 541–547 (1995).
11. Walunas, T. L. et al. CTLA-4 can function as a negative regulator of T cell activation. *Immunity* **1**, 405–413 (1994).
12. Bachmann, M. F., Kohler, G., Ecabert, B., Mak, T. W. & Kopf, M. Cutting edge: lymphoproliferative disease in the absence of CTLA-4 is not T cell autonomous. *J. Immunol.* **163**, 1128–1131 (1999).
13. Qureshi, O. S. et al. Trans-endocytosis of CD80 and CD86: a molecular basis for the cell-extrinsic function of CTLA-4. *Science* **332**, 600–603 (2011).
14. Tekguc, M., Wing, J. B., Osaki, M., Long, J. & Sakaguchi, S. Treg-expressed CTLA-4 depletes CD80/CD86 by trogocytosis, releasing free PD-L1 on antigen-presenting cells. *Proc. Natl Acad. Sci. USA* https://doi.org/10.1073/pnas.2023739118 (2021).
15. Corse, E. & Allison, J. P. Cutting edge: CTLA-4 on effector T cells inhibits in trans. *J. Immunol.* **189**, 1123–1127 (2012).
16. Walker, L. S. & Sansom, D. M. The emerging role of CTLA4 as a cell-extrinsic regulator of T cell responses. *Nat. Rev. Immunol.* **11**, 852–863 (2011).
17. Benmebarek, M. R. et al. Killing mechanisms of chimeric antigen receptor (CAR) T cells. *Int. J. Mol. Sci.* https://doi.org/10.3390/ijms20061283 (2019).
18. Turtle, C. J. et al. Immunotherapy of non-Hodgkin's lymphoma with a defined ratio of $CD8^+$ and $CD4^+$ CD19-specific chimeric antigen receptor-modified T cells. *Sci. Transl. Med* **8**, 355ra116 (2016).
19. Grupp, S. A. et al. Chimeric antigen receptor-modified T cells for acute lymphoid leukemia. *N. Engl. J. Med* **368**, 1509–1518 (2013).
20. Xu, Y. et al. A novel antibody-TCR (AbTCR) platform combines Fab-based antigen recognition with γδ-TCR signaling to facilitate T-cell cytotoxicity with low cytokine release. *Cell Discov.* **4**, 62 (2018).
21. Wu, W. et al. Multiple signaling roles of CD3ε and its application in CAR-T cell therapy. *Cell* **182**, 855–871 (2020).
22. Gust, J. et al. Endothelial activation and blood–brain barrier disruption in neurotoxicity after adoptive immunotherapy with CD19 CAR-T cells neurotoxicity associated with CD19 CAR-T cells. *Cancer Discov.* **7**, 1404–1419 (2017).
23. Qureshi, O. S. et al. Constitutive clathrin-mediated endocytosis of CTLA-4 persists during T cell activation. *J. Biol. Chem.* **287**, 9429–9440 (2012).
24. Sansom, D. M. Moving CTLA-4 from the trash to recycling. *Science* **349**, 377–378 (2015).
25. Janman, D. et al. Regulation of CTLA-4 recycling by LRBA and Rab11. *Immunology* **164**, 106–119 (2021).
26. Gossen, M. & Bujard, H. Tight control of gene expression in mammalian cells by tetracycline-responsive promoters. *Proc. Natl Acad. Sci.* **89**, 5547–5551 (1992).
27. Kao, S. H. et al. Analysis of protein stability by the cycloheximide chase assay. *Bio. Protoc.* https://doi.org/10.21769/BioProtoc.1374 (2015).
28. Martínez-Martín, N. et al. T cell receptor internalization from the immunological synapse is mediated by TC21 and RhoG GTPase-dependent phagocytosis. *Immunity* **35**, 208–222 (2011).
29. Olson, M. L. et al. Low-affinity CAR T cells exhibit reduced trogocytosis, preventing rapid antigen loss, and increasing CAR T cell expansion. *Leukemia* **36**, 1943–1946 (2022).
30. Bloemberg, D. et al. A high-throughput method for characterizing novel chimeric antigen receptors in Jurkat cells. *Mol. Ther. Methods Clin. Dev.* **16**, 238–254 (2020).
31. Krammer, P. H. CD95's deadly mission in the immune system. *Nature* **407**, 789–795 (2000).
32. Huang, F. L., Liao, E. C., Li, C. L., Yen, C. Y. & Yu, S. J. Pathogenesis of pediatric B-cell acute lymphoblastic leukemia: molecular pathways and disease treatments. *Oncol. Lett.* **20**, 448–454 (2020).
33. Gomes-Silva, D. et al. Tonic 4-1BB costimulation in chimeric antigen receptors impedes T cell survival and is vector-dependent. *Cell Rep.* **21**, 17–26 (2017).
34. Long, A. H. et al. 4-1BB costimulation ameliorates T cell exhaustion induced by tonic signaling of chimeric antigen receptors. *Nat. Med.* **21**, 581–590 (2015).
35. Lee, P. H. et al. Host conditioning with IL-1β improves the antitumor function of adoptively transferred T cells. *J. Exp. Med.* **216**, 2619–2634 (2019).
36. Velica, P. et al. Modified hypoxia-inducible factor expression in CD8(+) T cells increases antitumor efficacy. *Cancer Immunol. Res.* **9**, 401–414 (2021).
37. Maus, M. V. CD19 CAR T cells for adults with relapsed or refractory acute lymphoblastic leukaemia. *Lancet* **398**, 466–467 (2021).
38. Li, Y. et al. KIR-based inhibitory CARs overcome CAR-NK cell trogocytosis-mediated fratricide and tumor escape. *Nat. Med.* **28**, 2133–2144 (2022).
39. Li, G. et al. T cell antigen discovery via trogocytosis. *Nat. Methods* **16**, 183–190 (2019).
40. Stojanovic, A., Fiegler, N., Brunner-Weinzierl, M. & Cerwenka, A. CTLA-4 is expressed by activated mouse NK cells and inhibits NK cell IFN-γ production in response to mature dendritic cells. *J. Immunol.* **192**, 4184–4191 (2014).
41. Lougaris, V. et al. CTLA-4 regulates human natural killer cell effector functions. *Clin. Immunol.* **194**, 43–45 (2018).
42. Philip, M. et al. Chromatin states define tumour-specific T cell dysfunction and reprogramming. *Nature* **545**, 452–456 (2017).
43. Caruso, H. G. et al. Tuning sensitivity of CAR to EGFR density limits recognition of normal tissue while maintaining potent antitumor activity. *Cancer Res.* **75**, 3505–3518 (2015).
44. Ghorashian, S. et al. Enhanced CAR T cell expansion and prolonged persistence in pediatric patients with ALL treated with a low-affinity CD19 CAR. *Nat. Med.* **25**, 1408–1414 (2019).

45. Rodriguez-Marquez, P. et al. CAR density influences antitumoral efficacy of BCMA CAR T cells and correlates with clinical outcome. *Sci. Adv.* **8**, eabo0514 (2022).
46. Weber, E. W. et al. Transient rest restores functionality in exhausted CAR-T cells through epigenetic remodeling. *Science* https://doi.org/10.1126/science.aba1786 (2021).
47. Guo, T., Ma, D. & Lu, T. K. Sense-and-respond payload delivery using a novel antigen-inducible promoter improves suboptimal CAR-T activation. *ACS Synth. Biol.* **11**, 1440–1453 (2022).
48. Greenshpan, Y. et al. Synthetic promoters to induce immune-effectors into the tumor microenvironment. *Commun. Biol.* **4**, 143 (2021).

Methods

Institutional approval

All animal work was performed with the approval of Yale University Institutional Animal Care and Use Committee with approved protocols (Chen 2018-20068 and 2021-20068). All recombinant DNA and biosafety work were performed under the guidelines of Yale Environment, Health and Safety Committee with approved protocols (Chen-rDNA 15-45, 18-45, 21-45). All human sample work was performed under the guidelines of Yale University Institutional Review Board with an approved protocol (HIC no. 2000020784).

Vector construction

All lentivirus plasmids were generated by inserting target coding sequences into lentivirus transfer plasmid backbone (Addgene, #75112). Specifically, pLenti-EFS-Flag-m971-CD28-41BB-CD3zeta-T2A-mScarlet (CD22-CAR) was generated by amplifying the sequence from a gblock synthesized by IDT and inserting it into the lentiviral backbone using Gibson Assembly. To generate CAR-CCT constructs, 1CCT, 2CCT and 3CCT were inserted immediately before the T2A sequences, by amplifying 1–3 CCTs from the synthesized sequences with three tandem CCTs. mCMV-CAR was generated by replacing the EFS promoter in the CD22-CAR with a minimal CMV promoter using Gibson Assembly. CD19-CAR and CD19-CAR-CCT constructs were generated by replacing the m971 single-chain variable fragment (scFv) with the FMC63 scFv from the above-mentioned CD22-CAR construct. Similar methods were used to generate pLenti-EFS-CD22-GGGGS-mTagBFP and pLenti-EFS-CD22-GGGGS-eGFP constructs.

Cell culture

The 293T, NALM6 and Jurkat cells were purchased from the ATCC. Human peripheral blood mononuclear cells (PBMCs) were purchased from STEMCELL Technologies. NALM6 expressing GFP-luciferase (NALM6GL) was previously generated in the laboratory[49]. The 293T cells were cultured in DMEM (Gibco) with 10% FBS (Corning) and 200 U ml^{-1} penicillin–streptomycin (Gibco), hereafter referred to as cDMEM. NALM6 cells and Jurkat cells were cultured in RPMI-1640 (Gibco) medium supplemented with 10% FBS and 200 U ml^{-1} penicillin–streptomycin, hereafter referred to as cRPMI. Human PBMCs were cultured in X-VIVO 15 medium (Lonza) supplied with 5% human AB serum (MP Biomedical) and 10 ng ml^{-1} human IL-2 (Peprotech), hereafter referred to as cX-VIVO. All cells were grown at 37 °C and 5% CO_2 with saturating humidity.

Lentivirus production

The 40 million 293T cells (passage number <20) were seeded onto a 150-mm dish. The next day, the medium was replaced with pre-warmed fresh cDMEM. In total, 20 µg transfer plasmid, 10 µg psPAX2 (Addgene) and 5 µg pMD2.G (Addgene) were diluted with 1 ml plain DMEM. In a separate tube, 87.5 µl LipoD293 was diluted with 1 ml plain DMEM and then added to the diluted DNA mixture. This transfection mix was then briefly vortexed and incubated at room temperature for 15 min before being added to the 293T cells. Supernatant was collected 48 h later, spun down at 3,000*g* for 15 min, concentrated by adding 40% (w/v) PEG8000 directly to the supernatant to final concentration of 8% (w/v) PEG8000 and then incubated at 4 °C overnight. The lentivirus was spun down at 1,500*g* for 30 min and resuspended with 1 ml fresh cRPMI or cX-VIVO medium. The virus was stored at −80 °C before usage.

Generation of stable cell lines

All stable cell lines were generated by lentiviral infection and purified based on reporter gene (GFP, BFP or mScarlet) expression using flow cytometer. NALM6-CD22-GFP cells were generated with a lentiviral vector that expressed full-length human CD22 and eGFP linked by a GGGGS linker. NALM6GL-CD22-BFP cells were generated using a similar lentiviral construct, where eGFP was swapped for mTagBFP in NALM6GL cells. CAR-Jurkat cells were generated by transducing Jurkat cells using the same lentiviral constructs shown in Extended Data Fig. 1a.

Human T cell isolation and culture

Human $CD3^+$ T cells were isolated directly from PBMC samples by using magnetic positive selection. Briefly, 15 million PBMCs were labeled with anti-human CD3-biotin (BioLegend, 1:100 dilution) in MACS buffer (PBS supplemented with 0.5% BSA and 2 mM EDTA) at 4 °C for 10 min. After washing with MACS buffer, PBMCs were resuspended with 120 µl MACS buffer and stained with 30 µl anti-biotin beads (Miltenyi) at 4 °C for 15 min. Labeled $CD3^+$ T cells were separated by using MACS LS Columns (Miltenyi) and MACS Separators (Miltenyi) according to the manufacturer's instructions. Purified $CD3^+$ T cells were cultured in cX-VIVO medium and stimulated with Dynabeads Human T-Activator CD3/CD28 (Thermo Fisher Scientific) at a bead-to-cell ratio of 1:1 for 24 h before being infected with lentiviruses.

Human T cell transduction with lentivirus

Human $CD3^+$ T cells activated for 24 h were collected and resuspended with concentrated lentiviruses, supplemented with 8 µg ml^{-1} polybrene, at a concentration of 1 million ml^{-1}. Cells were plated on a 24-well plate and spun at 2,000 r.p.m. (~900*g*) for 2 h at 37 °C. The virus supernatant was aspirated and replaced with fresh cX-VIVO medium. Cells were split 1 to 2 every other day and transduction was checked 4 d after infection by flow cytometry. CAR-T cells were sorted on day 7 based on mScarlet expression and expanded in vitro for another 7 d before being used for in vitro and in vivo experiments.

Antibody and staining for flow cytometry

All antibodies used in this study are listed in the Antibodies section of the Nature Portfolio Reporting Summary. Cell surface antigens were stained with indicated antibody cocktails in MACS buffer on ice for 15 min as indicated in the figure legend. To stain endocytic CAR or cycling CTLA-4, CAR-T cells were stained using anti-Flag-BV421 (rat-IgG2a, BioLegend, 1:500 dilution) or anti-CTLA-4-APC (mouse IgG2a, BioLegend, 1:200 dilution) at 37 °C for 1 h, followed by washing with ice-cold MACS buffer. Those cells were then stained with anti-rat-IgG2a-Alexa Fluor 647 (BioLegend, 1:500 dilution) or anti-mouse IgG2a-BV421 (BioLegend, 1:500 dilution) at 4 °C for 15 min before running on the flow cytometer. To quantify apoptosis, cells were stained with annexin V Pacific-blue conjugates (Thermo Fisher) in annexin V binding buffer (BD) at room temperature for 15 min and immediately analyzed by flow cytometer. LIVE/DEAD Fixable Near-IR Dead Cell Stain (Invitrogen) was included for all staining to exclude unspecific staining of dead cells. Samples were collected or sorted on a four-laser (405 nm, 488 nm, 561 nm and 640 nm) Aria II cell sorter (BD). For sorting experiments, sorting purity was checked after every sort to make certain it was higher than 95%. All flow cytometry data were analyzed using FlowJo software v.10.8.0 (BD).

In vitro CAR-T killing assay

Variable amounts of purified CAR-T cells were cultured with fixed amount of NALM6GL cells at an E:T ratio of 1:2, 1:4 or 1:8 in a 96-well U-bottom plate. 24 h later, cells were either collected for flow cytometry analysis or re-stimulated with the same amount of NALM6GL cells as used in the first-round co-culture. 24 or 48 h later, NALM6GL cells and CAR-T cells were stained with indicated antibody cocktails. Cell counting beads (BioLegend) were added to all samples for absolute cell number measurement. For multiplex cytokine detection, the supernatant from cocultures was collected and measured by LEGENDplex Human CD8/NK Panel (BioLegend).

Proliferation assay

Purified CAR-T cells were stained in PBS with 10 µM Cell Proliferation Dye eFluor 450 (Thermo Fisher) at 37 °C for 5 min. Cells were then

washed three times with cRPMI medium and resuspended in cX-VIVO medium at a final concentration of 0.5 million ml^{-1}. Then, 200 µl cells were seeded into a 96-well U-bottom plate. After 4 d, eFluor450 dilution was measured by flow cytometry.

Measurement of phosphorylation and cytokine production

To measure phospho-ERK, CAR-T cells were first starved overnight in serum free X-VIVO medium and stained for LIVE/DEAD Fixable Near-IR Dead Cell Stain (Invitrogen). After washing with ice-cold PBS, those CAR-T cells were incubated with 2 µg ml^{-1} biotinylated human CD22 (ECD) on ice for 30 min. Signal transduction was induced by crosslinking with 10 µg ml^{-1} streptavidin (BioLegend) at 37 °C for 5 min. Crosslinking was stopped immediately with the Phosflow Fix Buffer I (BD) and fixed at 37 °C for 10 min. After this, cells were permeabilized with BD Phosflow Perm Buffer III on ice for 30 min, followed by anti-ERK1/2 (pT202/pY204)-Alexa Fluor 647 (BioLegend) staining at room temperature for 30 min. For the intracellular IFN-γ and TNF-α staining, CAR-T cells were co-cultured with NALM6GL cells at the indicated E:T ratio for 4 h with the presence of 1× brefeldin A (BioLegend). Cells were first stained with the Live/Dead-Near-IR dye before fixed, permeabilized and stained with a BD Cytofix/Cytoperm Buffer System.

Measurement of CAR endocytosis rate

A previously described method was used[23]. Briefly, CAR-T cells were first stained with anti-Flag (BioLegend) at 4 °C for 15 min and washed with ice-cold MACS buffer. Those cells were then resuspended with cX-VIVO medium and incubated at 37 °C for 0, 10, 20 or 30 min to allow endocytosis. Following incubation, CAR-T cells were washed with ice-cold MACS buffer. CAR molecules that remained on the cell surface were stained with an anti-rat-IgG2a-Alexa Fluor 647 secondary antibody at 4 °C for 15 min. The decrease in the percentage of cells staining positive for the secondary antibody was quantified by flow cytometry as an indication of endocytosis rate.

Measurement of recycling CAR or CTLA-4

A previously described method was used[25]. Briefly, CAR-T cells were first stained with anti-Flag (BioLegend) or anti-CTLA-4 (BioLegend) at 37 °C for 1 h and washed with ice-cold MACS buffer. The secondary antibody either stained at 4 °C for 15 min (baseline) or at 37 °C for 30 min or 60 min to see an increase in the secondary antibody signal when compared to the baseline. The increase (fold change) in the percentage of cells staining positive for the secondary antibody was quantified by flow cytometry as an indication of recycling.

Cycloheximide chase assay

CAR-T cells were treated with 50 µg ml^{-1} cycloheximide (Sigma) at 37 °C for up to 4 h. Total CAR expression was quantified by staining intracellular Flag expression using BD Cytofix/Cytoperm Buffer System.

CAR degradation with antibody feeding

A previously described method was used[25]. Briefly, CAR-T cells were incubated with anti-Flag (BioLegend) at 37 °C for 1 h. Cells were then washed and incubated at 37 °C for up to 4 h with or without 10 µM bortezomib (Sigma) or 10 nM BafA1. Cells were then fixed and permeabilized with BD Cytofix/Cytoperm Buffer System and stained with anti-rat-IgG2a-Alexa Fluor 647 before being analyzed by flow cytometry.

Quantification of CD22 transfer by confocal microscopy

About 10,000 purified CAR-T cells that had performed trogocytosis ($mScarlet^+BFP^+$) were seeded onto a µ-slide eight-well glass-bottom chamber (Ibidi) that had been previously treated with poly-L-lysine. Cells were then stained with deep red CellMask Plasma Membrane dye (Thermo Fisher) at 37 °C for 5 min according to the manufacturer's instruction. Cells were imaged by Leica Stellaris 8 FALCON with the ×40 objective (oil). Representative images were exported using ImageJ (https://imagej.nih.gov/). The percentage of CD22 membrane colocalization was analyzed by a customized MATLAB (MathWorks) app (https://github.com/xs254/Colocalization_calculator/tree/main) with standard parameters. Antigen-membrane colocalization percentage was calculated by the following formula, where $I_{antigen-cytosol}$, $I_{antigen-cell}$ stands for intensity of each pixel classified as foreground in both the antigen and cytosol mask, respectively. $I_{antigen\ background}$ stands for mean intensity of background pixels in the antigen image (2.5 used for all analysis).

$$p_{colocalization} = 1 - \frac{\sum(I_{antigen-cytosol} - I_{antigen\ background})}{\sum(I_{antigen-cell} - I_{antigen\ background})}$$

Timelapse live cell imaging of trogocytosis and fratricide

The 40,000 CAR-T cells and NALM6GL-CD22-BFP cells were seeded at an E:T ratio of 2:1 into a µ-slide eight-well glass-bottom chamber (Ibidi) that had been previously treated with 7.5 µg cm^{-2} poly-L-lysine (Sigma). Then, 5 nM SYTOX Deep Red Nucleic Acid Stain (Thermo Fisher) was supplemented into the culture to allow for dead cell staining. Cells were imaged with a Leica Stellaris 8 FALCON with the ×40 objective (oil) in the live cell imaging chamber at 37 °C and 5% CO_2. A 4 × 4 field of view was taken at a scan interval of every 3–5 min for up to 8 h. Images were processed and exported through ImageJ (https://imagej.nih.gov/).

Trogocytosis assay

CAR-T or CAR-Jurkat cells were co-cultured with NALM6GL, NALM6GL-CD22-BFP or NALM6-CD22-GFP cells for the indicated times at a fixed E:T ratio. Trogocytosis of CD22 by CAR-T cells was quantified by measuring CD22 using an antibody, BFP or GFP signal. For trogocytosis inhibition, as indicated in figure legends, CAR-T cells were pretreated with 1 µM latrunculin A (Sigma-Aldrich) at 37 °C for 15 min before co-incubation with target cells.

Degranulation assay

CAR-Jurkat cells were co-cultured with NALM6-CD22-GFP at an E:T ratio of 1:1 for 4 h to allow for CD22-GFP transfer from NALM6 to CAR-Jurkat cells. Both $Trog^+$ CAR-Jurakt and $Trog^-$ CAR-Jurkat cells were sorted out based on their expression of CD22-GFP using an AriaII sorter (BD). Those cells were then used as target cells and co-cultured for 2 h with fresh CAR-T cells that had been labeled with 10 nM eFluor450 to allow for differentiation between CAR-T and CAR-Jurkat cells. Variable CAR-T to CAR-Jurkat ratios were used as indicated in figure legends. Anti-CD107-APC (BioLegend) and 1× Monensin (BioLegend) were added into the culture during the incubation. Cells were then stained with LIVE/DEAD Fixable Near-IR Dead Cell Stain (Invitrogen) before being analyzed by flow cytometry.

Bulk RNA sequencing and data processing

To profile baseline differences, purified CAR-T cells expanded in vitro for 14 d were collected. To profile differences under repeated stimulations, CAR-T cells expanded in vitro for 14 d were co-cultured with NALM6GL cells at E:T of 1:2, followed by a second round of NALM6GL cell stimulation 24 h after the initial co-culture. $mScarlet^+$ CAR-T cells were sorted 72 h after the initial co-culture and were lysed for bulk RNA extraction using an RNeasy Plus mini isolation kit (QIAGEN). Library preparations were performed using a NEBNext Ultra RNA Library Prep kit for Illumina according to the manufacturer's instructions. Samples were barcoded and multiplexed using NEBNext Multiplex Oligos for Illumina (index primers set 1). Libraries were then sequenced with NovaSeq (Illumina). Fastq files generated by sequencing were aligned and mapped using STAR[50] with the human genome assembly v.GRCh38. Differential expression was analyzed using DEseq2 (ref. 51). $P_{adj} < 0.01$ and $|\log_2 foldchange| > 1$ were set as the cutoff for determining DEGs, which were selected for over representation analysis using

the R package enrichplot[52]. Visualizations of DEGs, such as volcano plots and heat maps, were generated using standard R packages such as pheatmap and VennDiagram.

Measurement of relative CAR-T survival

CAR, CAR-1CCT, CAR-2CCT and CAR-3CCT cells stained with 1 µM eFluor450 were mixed with CAR-T cells stained with 10 µM eFluor450 at a 1:1 ratio. For in vitro measurement, these mixed cells were then cultured with or without NALM6GL stimulation at an E:T of 1:2 for 24 h. For in vivo measurement, NOD.Cg-Prkdc^{scid}Il2rg^{tm1Wjl}/SzJ (NSG) mice were first inoculated with 1 million NALM6GL cells intravenously (i.v.) on day 0. A mixture of 2 million labeled cells was transferred to the leukemia NSG models on day 4. Bone-marrow samples were collected and processed into a single-cell suspension 1 d later. Cells were stained using LIVE/DEAD Fixable Near-IR Dead Cell Stain (Invitrogen) and anti-human CD22 APC (BioLegend) before being analyzed by flow cytometer, which was used to determine the relative percentage of eFluor450^{low} and eFluor450^{high} populations. The relative survival of CAR-T cells was calculated by the following equation: relative survival (%) = $((l_w{:}h_w) - (l_{wo}{:}h_{wo}))/(l_{wo}{:}h_{wo}) \times 100\%$, in which l_w and h_w represent the percentage of eFluor450 low and high populations, respectively, with NALM6GL cell stimulation (in vitro assays) or after transfer (in vivo assays) and l_{wo} and h_{wo} represent the percentage of eFluor450 low and high populations, respectively, without NALM6GL cell stimulation (in vitro assays) or before transfer (in vivo assays).

In vivo evaluation of CAR-T performance

NSG mice were purchased from the Jackson Laboratory and bred in house. NSG mice (female, 6–10 weeks old) were inoculated with 0.5 million NALM6GL cells intravenously (i.v.) on day 0 and treated with 1 million CAR-T cells (i.v.) on day 4. Relapse was modeled by re-challenging all mice with 0.5 million NALM6GL cells (i.v.) on day 12. To better model the clinical response to CAR-T cells in NSG mice[53], 2.5 µg human recombinant IL-2 (Peprotech) was administered subcutaneously (s.c.) every day starting on day 4 for 24 d. Disease progression was monitored by bioluminescence imaging and survival analysis. For the in vivo phenotyping, 2.5 µg human recombinant IL-2 was administered s.c. every day from day 4 to day 14. All mice were killed on day 15. Spleen and BM tissues were collected. For preparations, spleens were prepared by mashing them through 100-µm filters. For bone-marrow isolation, femurs with both ends cut by scissors were isolated and bone marrow was flushed out with 2 ml cRPMI using a 25G needle. Red blood cells were lysed with ACK Lysis Buffer (Lonza), incubated for 2 min at room temperature and washed with cRPMI. Lymphocytes were poured through a 40-µm filter before staining with antibody cocktail. Cell counting beads (BioLegend) were added to all samples for absolute cell number measurement by Aria II cell sorter (BD).

scRNA-seq library preparation, sequencing and data analysis

Live CAR-T cells were sorted based on mScarlet expression from spleen and BM and processed as described above. For all four groups, samples from three individual mice within the same group were pooled together to minimize sampling bias. Sorted cells were washed with PBS. Cell number and viability were assessed by Trypan blue (Lonza) staining. Approximately 2,000–10,000 purified mScarlet$^+$ cells were used for scRNA-seq library preparation using Chromium Next GEM Single Cell 5′ Reagent kits V2 (10x Genomics) according to the manufacturer's instructions. The single-cell libraries were sequenced by NovaSeq 6000 (Illumina) with a 2 × 150 bp. Analysis of scRNA-seq was performed using standard pipelines with custom codes. Briefly, raw FASTQ data were pre-processed with CellRanger v.6.0.1. The processed data matrices were analyzed and visualized using the Seurat v.4 package[54]. Specifically, the dataset was filtered to retain cells with <10% mitochondrial counts and 200–2,500 unique expressed features[55]. The dataset was then log-normalized, scaled using the reciprocal-PCA dimensional reduction with 2,000 anchors[56]. Dimensional reduction was performed by UMAP[57] using the first ten dimensions from PCA. Cells were clustered in low-dimensional space by generating a shared nearest neighbor graph (k = 20, first ten PCs). Each cell cluster was annotated by canonical marker genes. An empirical resolution (0.2), followed by a second-step resolution for sub-clustering, was chosen for better separation of CD4$^+$ and CD8$^+$ T cell populations.

Statistics and schematic illustrations

Statistics for standard biological assays were conducted using Prism, with detailed methods indicated in figure legends. Schematic illustrations were created with Affinity Designer.

Reporting summary

Further information on research design is available in the Nature Portfolio Reporting Summary linked to this article.

Data availability

All data generated or analyzed during this study are provided. Source data and statistics are provided in an Excel file in Supplementary Table 3. Processed data for genomic sequencing and gene expression are provided as processed quantifications in Supplementary Tables 1 and 2. Genomic sequencing raw data are deposited at the Gene Expression Omnibus under accession no. GSE234307. Source data are provided with this paper.

Code availability

The code used for data analysis and the generation of figures related to this study can be accessed from GitHub at https://github.com/Ariel-Xiaoyu/CAR-CCT.

References

49. Dai, X. et al. One-step generation of modular CAR-T cells with AAV-Cpf1. *Nat. Methods* **16**, 247–254 (2019).
50. Dobin, A. et al. STAR: ultrafast universal RNA-seq aligner. *Bioinformatics* **29**, 15–21 (2013).
51. Love, M. I., Huber, W. & Anders, S. Moderated estimation of fold change and dispersion for RNA-seq data with DESeq2. *Genome Biol.* **15**, 550 (2014).
52. Yu, G. enrichplot: Visualization of Functional Enrichment Result. R package v.1.8.1. https://github.com/GuangchuangYu/enrichplot (2020).
53. Jespersen, H. et al. Clinical responses to adoptive T-cell transfer can be modeled in an autologous immune-humanized mouse model. *Nat. Commun.* **8**, 707 (2017).
54. Satija, R., Farrell, J. A., Gennert, D., Schier, A. F. & Regev, A. Spatial reconstruction of single-cell gene expression data. *Nat. Biotechnol.* **33**, 495–502 (2015).
55. Jordao, M. J. C. et al. Single-cell profiling identifies myeloid cell subsets with distinct fates during neuroinflammation. *Science* **363**, 365–36 (2019).
56. Stuart, T. et al. Comprehensive integration of single-cell data. *Cell* **177**, 1888–1902 (2019).
57. Becht, E. et al. Dimensionality reduction for visualizing single-cell data using UMAP. *Nat. Biotechnol.* https://doi.org/10.1038/nbt.4314 (2018).

Acknowledgements

We thank Drs Krause, Isufi and Bersenev for discussions on cell therapy. We thank all members of the Chen laboratory, as well as various colleagues and core facility staff at Yale for assistance and/or discussions. We thank staff at the Yale West Campus Imaging Core for their support and assistance in this work. We thank R. Glen for

helpful proofreading of the manuscript. S.C. is supported by Yale SBI/Genetics Startup Fund, National Institutes of Health (NIH)/National Cancer Institute/National Institute on Drug Abuse (DP2CA238295, R01CA231112, U54CA209992-8697, R33CA225498 and RF1DA048811), U.S. Department of Defense (DOD) (W81XWH-17-1-0235, W81XWH-20-1-0072, W81XWH-21-1-0514), Cancer Research Institute (CLIP), the American Association for Cancer Research (499395, 17-20-01-CHEN), Alliance for Cancer Gene Therapy, Sontag Foundation (DSA), Pershing Square Sohn Cancer Research Alliance, Dexter Lu, Ludwig Family Foundation, Blavatnik Family Foundation and Chenevert Family Foundation. P.A.R. is supported by an NIH training grant (T32GM007499) and a Lo Fellowship. M.B.D. is supported by an NIH training grant (T32GM007205). R.D.C. is supported by an NIH MSTP training grant (T32GM007205) and National Research Service Award fellowship (F30CA250249).

Author contributions

X.Z. designed experiments with discussion with H.C., M.B.D. and R.D.C. X.Z. and H.C. performed most of the experiments. S.Y.F., M.M., M.B. and M.B.D. assisted with the experiments. X.Z. analyzed the high-throughput data. R.D.C., P.A.R., K.T. and K.S. assisted with data analysis. A.L. and X.S. assisted with imaging analysis. X.Z. conceived the study with high-level input from S.C. S.C. secured funding and supervised the work. X.Z., H.C., R.D.C. and S.C. prepared the paper with input from all authors.

Competing interests

A patent was filed by Yale University regarding the data in this study (inventors S.C. and X.Z.), which was licensed to Cellinfinity Bio, a Yale biotech startup founded by S.C. S.C. is also a (co)founder of EvolveImmune, NumericGlobal, Chen Tech and Chen Consulting, all unrelated to this study. All other authors have no competing interests.

Additional information

Extended data is available for this paper at https://doi.org/10.1038/s41590-023-01571-5.

Supplementary information The online version contains supplementary material available at https://doi.org/10.1038/s41590-023-01571-5.

Correspondence and requests for materials should be addressed to Sidi Chen.

Peer review information *Nature Immunology* thanks the anonymous reviewers for their contribution to the peer review of this work. Primary Handling Editor: Stephanie Houston, in collaboration with the *Nature Immunology* team. Peer reviewer reports are available.

https://doi.org/10.1038/s41590-023-01571-5

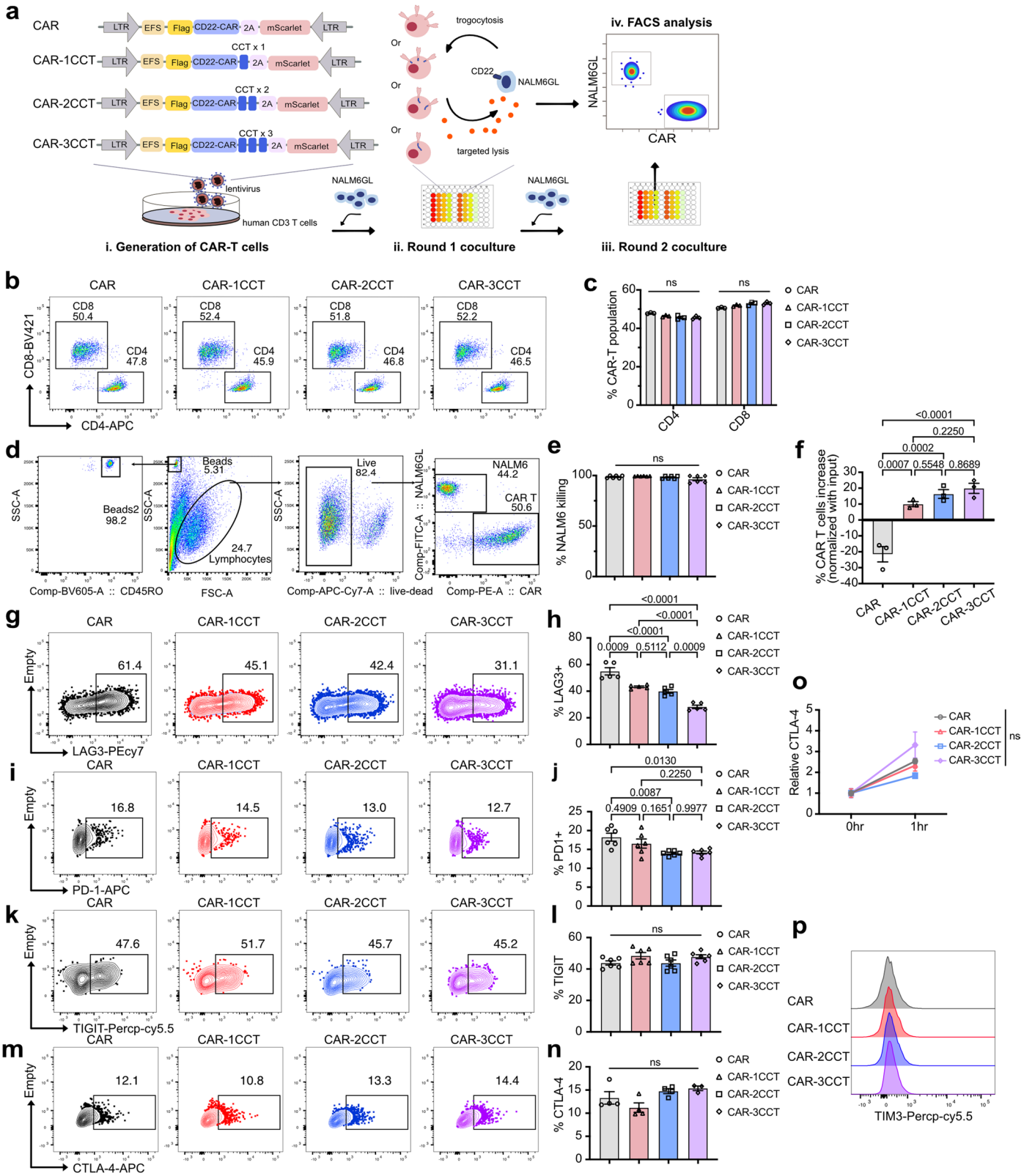

Extended Data Fig. 1 | See next page for caption.

https://doi.org/10.1038/s41590-023-01571-5

Extended Data Fig. 1 | Characterization of CAR-T cells with CCT fusion after one round stimulation with NALM6GL cells. a. Schematics of the workflow used to generate CAR-T cells for effector function assessment *in vitro*. (i) Generation of CAR-T cells. Human CD3 T cells were infected by lentiviruses carrying CAR targeting human CD22 (m971-CD28-41BB-CD3zeta). These CARs were engineered with either monomeric (CAR-1CCT), duplex (CAR-2CCT) or triplex CCTs (CAR-3CCT) fused to the C terminus of human CD22-CAR (CAR), followed by a fluorescent reporter mScarlet, separated by T2A sequences. Flag sequences were tagged at N-terminal of the CAR for surface expression detection. (ii) Round 1 co-culture. Those four groups of CAR-T cells generated in step (i) were co-culture with NALM6GL cells at variable E/T ratios for 24 hours. (iii) Round 2 co-culture. An additional round of NALM6GL cells were supplemented into the initial co-culture for 24 hours. (iv). FACS analysis. Cells from both round1 and 2 cocultures were quantified by fluorescence-activated single cell sorting (FACS). **b**. Representative flow cytometry results showing CD4 and CD8 staining of CAR-T cells 7 days after transduced with CAR-T constructs. **c**. Quantification of (**b**). showing the CD4 and CD8 percentage of CAR-T cells, n = 3. **d**. Representative flow cytometry results showing the gating strategy used in Fig. 1a–d. **e**. Quantification of NALM6 killing by CAR-T cells. Purified CAR-T cells were co-cultured with one round of NALM6GL cells at E/T = 1/2 for 24 hours, n = 6. **f**. Quantification of the increases in CAR-T cell counts after one round of NALM6GL stimulation, n = 3. **g**-**p**. Representative flow cytometry analysis and quantification of LAG3 (**g**,**h**), PD-1(**i**,**j**), TIGIT(**k**,**l**), cycling CTLA-4(**m**,**n**), recycling CTLA-4 (**o**) and TIM3 (**p**) on CAR-T cells after stimulated with NALM6GL cells at E/T = 1/2 for 24 hours. For all bar plots, data are shown as mean ± s.e.m. One-way ANOVA with Dunnett's multiple-comparisons test is used to assess significance for figure (**e**), (**f**), (**h**), (**j**), (**l**) and (**n**). Two-way ANOVA with Tukey's multiple-comparisons test is used to assess significance for (**c**) and (**o**). ns = $p > 0.05$. Exact p values are labeled. All numbers defined by 'n' indicate the number of biologically independent samples. Data are representative of three independent experiments performed with biological repeats.

https://doi.org/10.1038/s41590-023-01571-5

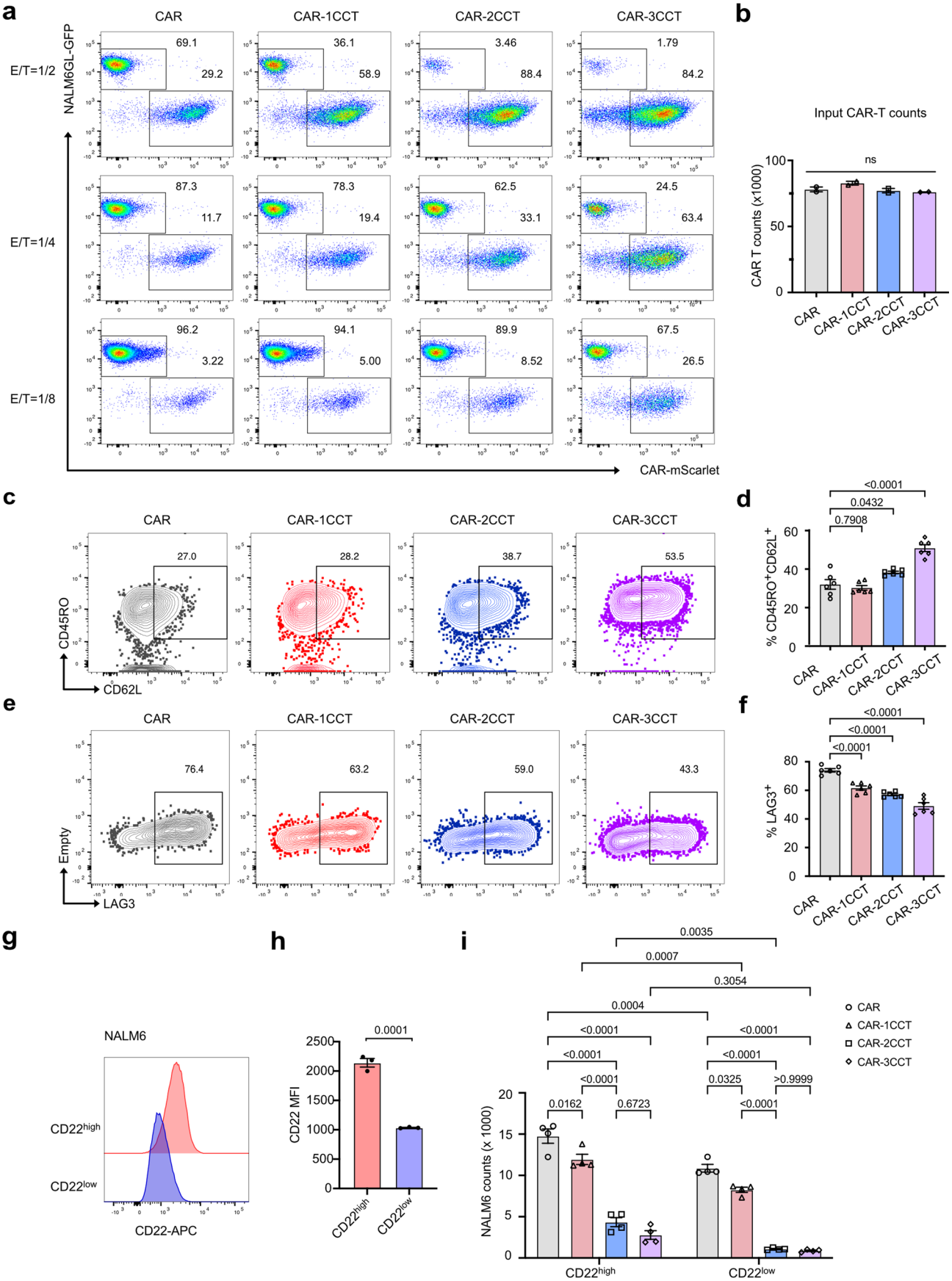

Extended Data Fig. 2 | See next page for caption.

https://doi.org/10.1038/s41590-023-01571-5

Extended Data Fig. 2 | CCT fusion enhanced CAR-T killing under repeated stimulation. a. Representative flow cytometry analysis for Fig. 1a–d showing CAR-T killing capability under two rounds of NALM6GL stimulation. **b**. Quantification of input CAR-T cell counts without NALM6GL stimulation showing relatively equal amount of input CAR-T cells, n = 2, ns = $p > 0.05$. **c**. Representative flow cytometry results showing the differentiation stage, indicating by the expression of CD45RO and CD62L, of CAR-T cells after two rounds of co-culture with NALM6GL cells. **d**. Quantification of **c**. showing the $CD45RO^+$ $CD62L^+$ CAR-T cells in percentage, n = 6. **e**. Representative flow cytometry results showing the expression level of LAG3 on CAR-T cells after being stimulated with two rounds of NALM6GL. **f**. Quantification of (**e**) showing the $LAG3^+$ CAR-T cells in percentage, n = 6. **g**. Representative flow cytometry analysis on the CD22 expression level of $CD22^{high}$ and $CD22^{low}$ NALM6 cells. **h**. Quantification of (**g**) showing CD22 MFI of $CD22^{high}$ and $CD22^{low}$ NALM6 cells, n = 3. **i**. Quantification of live NALM6 cell count after two rounds of coculturing with CAR-T cells at E/T = 1/2 by flow cytometry, n = 4. For all bar plot figures, data are shown as mean ± s.e.m. One-way ANOVA with Dunnett's multiple-comparisons test is used to assess significance. Exact *p* values are labeled. All numbers defined by 'n' indicate the number of biologically independent samples. Data are representative of three independent experiments performed with biological repeats.

https://doi.org/10.1038/s41590-023-01571-5

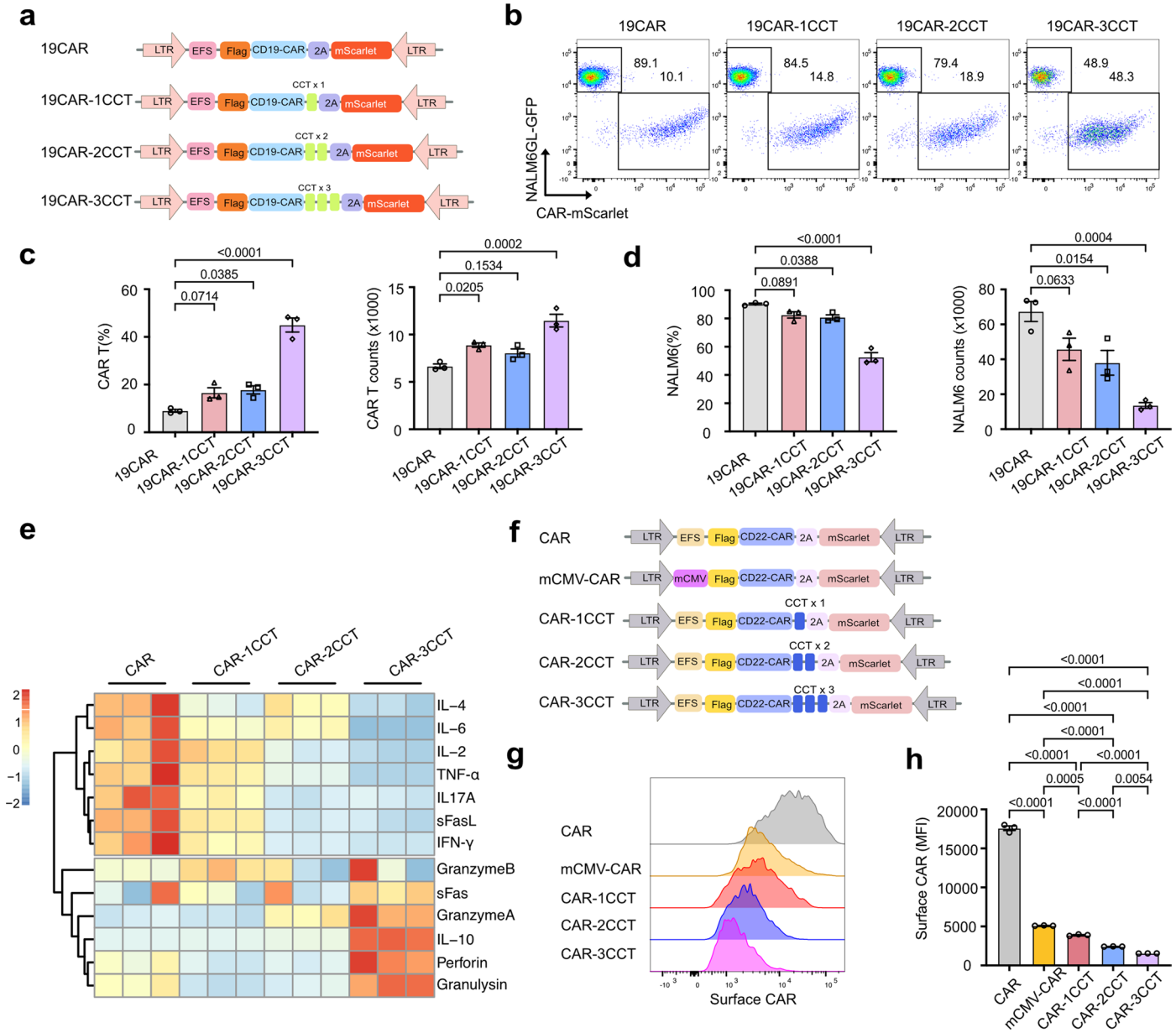

Extended Data Fig. 3 | CCT fusion enables enhanced killing with low production of proinflammatory cytokines. a. Schematics of lentiviral constructs to make CAR-T cells targeting human CD19 (FMC63-CD28-41BB-CD3zeta). CD19-CAR (19CAR) constructs were made by replacing the m971 scFv with the FMC63 scFv from Extended Data Fig. 1a. **b**. Representative flow cytometry analysis of 19CAR-T killing capability *in vitro*. **c**. Quantification of (**b**) showing CD19-CAR percentage (left panel), and counts (right panel), n = 3. **d**. Quantification of (**b**) showing NALM6GL percentage (left panel), and counts (right panel), n = 3. **e**. Quantification of 13 granule molecules and cytokines in CAR-T and NALM6GL cocultures. CAR-T cells were co-cultured with one round of NALM6GL cells at E/T = ½ for 24 hours. Co-culture supernatant was then collected and measured using LEGENDplex™ Human CD8/NK Panel, n = 3. **f**. Schematics of lentiviral constructs to make CD22 targeting CAR-T cells. In addition to the four constructs shown in Extended Data Fig. 1a, mCMV-CAR construct was generated by replacing the EFS promoter in the CAR construct with a minimal CMV promoter (mCMV). **g**. Representative flow cytometry analysis of CAR-T cells, pre-gated on mScarlet$^+$ populations, showing surface expression level of CAR, indicated by Flag staining. **h**. Quantification of (**g**) showing surface flag expression in MFI, n = 3. For all bar plot figures, data are shown as mean ± s.e.m. One-way ANOVA with Dunnett's multiple-comparisons test is used to assess significance. Exact *p* values are labeled. All numbers defined by 'n' indicate the number of biologically independent samples. Data are representative of two independent experiments performed with biological repeats.

https://doi.org/10.1038/s41590-023-01571-5

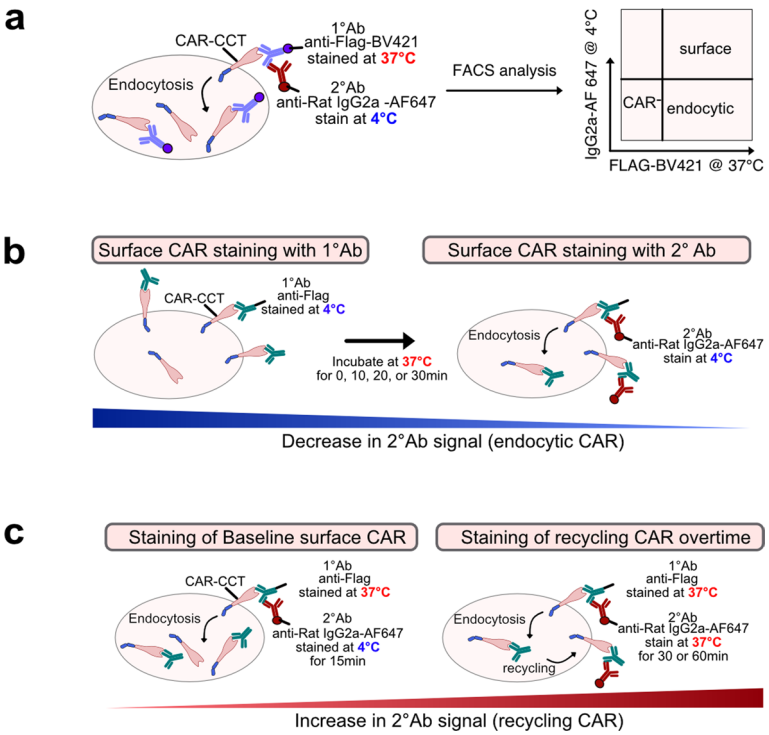

Extended Data Fig. 4 | Schematics of workflow of experiments for Fig. 2. a. Schematics of the workflow used in Fig. 2c, d for detecting CAR endocytosis. Surface and endocytic CAR were first stained with primary anti-Flag-BV421 at 37 °C for 30 minutes, followed by a secondary anti-Rat-IgG2a-AF647 stained at 4 °C for 15 minutes. The surface, endocytic CAR and CAR$^-$ populations were differentiated based on their staining patterns of the primary and secondary antibodies. **b.** Schematics of the workflow used in Fig. 2e to assess the endocytosis rate of CAR. Surface CAR was initially labeled with primary anti-Flag at 4 °C, followed by incubation of CAR-T cells at 37 °C for varying durations to allow endocytosis. The remaining surface-bound CAR molecules were then stained with a secondary anti-Rat-IgG2a-AF647 antibody at 4 °C. Endocytosis was quantified by the decrease in the percentage of cells stained positive for the secondary antibody. **c.** Schematics of the workflow used in Fig. 2f for detecting recycling CAR. Surface and endocytic CAR were first stained with primary anti-Flag at 37 °C for 30 minutes, followed by a secondary anti-Rat-IgG2a-AF647, either stained at 4 °C for 15 minutes (baseline) or at 37 °C for 30 minutes or 60 minutes. Recycling was quantified by the increase in the percentage of cells stained positive for the secondary antibody.

https://doi.org/10.1038/s41590-023-01571-5

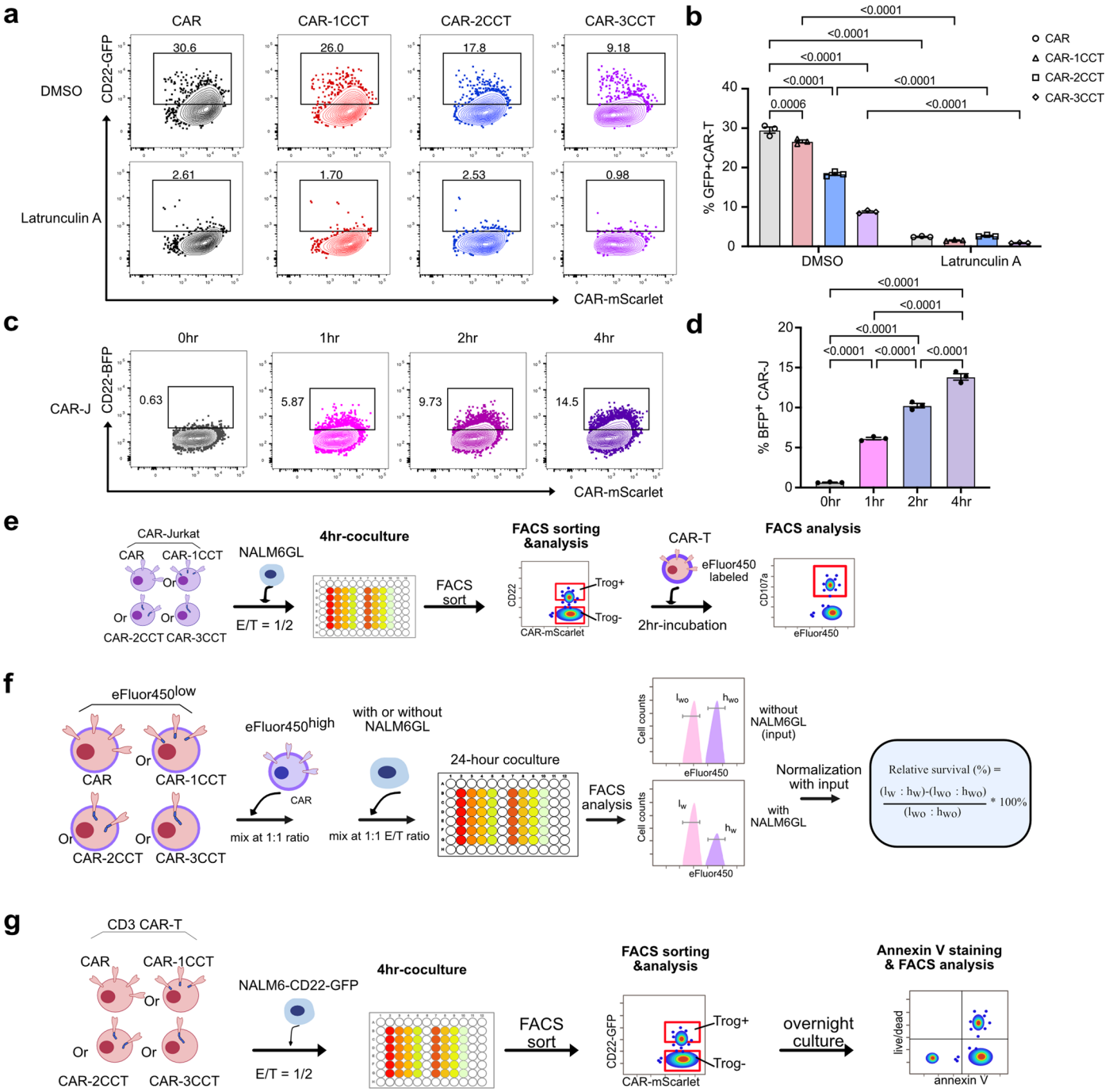

Extended Data Fig. 5 | CCT fusion decreased CAR-mediated trogocytosis. a. Representative flow cytometry analysis of CAR-mediated trogocytosis. CAR-T cells were pretreated with either DMSO (control) or 1 μM Latrunculin A at 37 °C for 15 min before co-cultured with NALM6-CD22-BFP cells for 2 hours. CD22-GFP transfer onto CAR-T cells were quantified by flow cytometry. **b.** Quantification of (**a**) showing the inhibition of CD22-GFP transfer by Latrunculin A, n = 3. **c.** Representative flow cytometry analysis of CAR-mediated trogocytosis by CAR-J cells. CAR-J cells co-cultured with NALM6GL-CD22-BFP cells for indicated time. CD22-BFP transfer onto CAR-T cells were quantified by flow cytometry. **d.** Quantification of (**c**) showing the transfer of CD22-BFP onto CAR-J cells, n = 3. **e.** Schematics of the workflow used in Fig. 3h, i for detecting the degranulation of CAR-T cells. CAR-Jurkat (CAR-J) cells were co-cultured with NALM6-CD22-GFP at an E/T ratio of 1:1 for 4 hours. Both Trog$^+$ CAR-J and Trog$^-$ CAR-J cells were sorted out based on their expression of CD22-GFP. Those cells were then co-cultured with eFluor450 labeled CAR-T cells for 2 hours for determine the expression of CD107a. **f.** Schematics of the CAR-T survival assay used in Fig. 4a–c. Control CAR-T cells labeled with 10 μM eFluor450 (eFluor450^{high}), were mixed 1:1 with CAR, CAR-1CCT, CAR-2CCT or CAR-3CCT cells labeled with 1 μM eFluor450 (eFluor450^{low}). These mixed CAR-T cells were then co-cultured with or without NALM6GL. Relative percentages of eFluor450 high and low populations gated from CAR$^+$ (mScarlet$^+$) cells were used for quantification of relative survival of CAR-T cells. **g.** Schematics of the workflow used in Fig. 4f, g. CAR-T cells were co-cultured with NALM6-CD22-GFP cells at E/T = 1/2 for 4 hours. Both Trog$^+$ CAR-T and Trog$^-$ CAR-T cells were sorted out based on their expression of CD22-GFP, and co-cultured separately overnight before staining for Annexin V. For all bar plot figures, data are shown as mean ± s.e.m. One-way ANOVA with Dunnett's multiple-comparisons test is used to assess significance for (**d**). Two-way ANOVA with Tukey's multiple-comparisons test is used to assess significance for (**b**). Exact *p* values are labeled. All numbers defined by 'n' indicate the number of biologically independent samples. Data are representative of two independent experiments performed with biological repeats.

https://doi.org/10.1038/s41590-023-01571-5

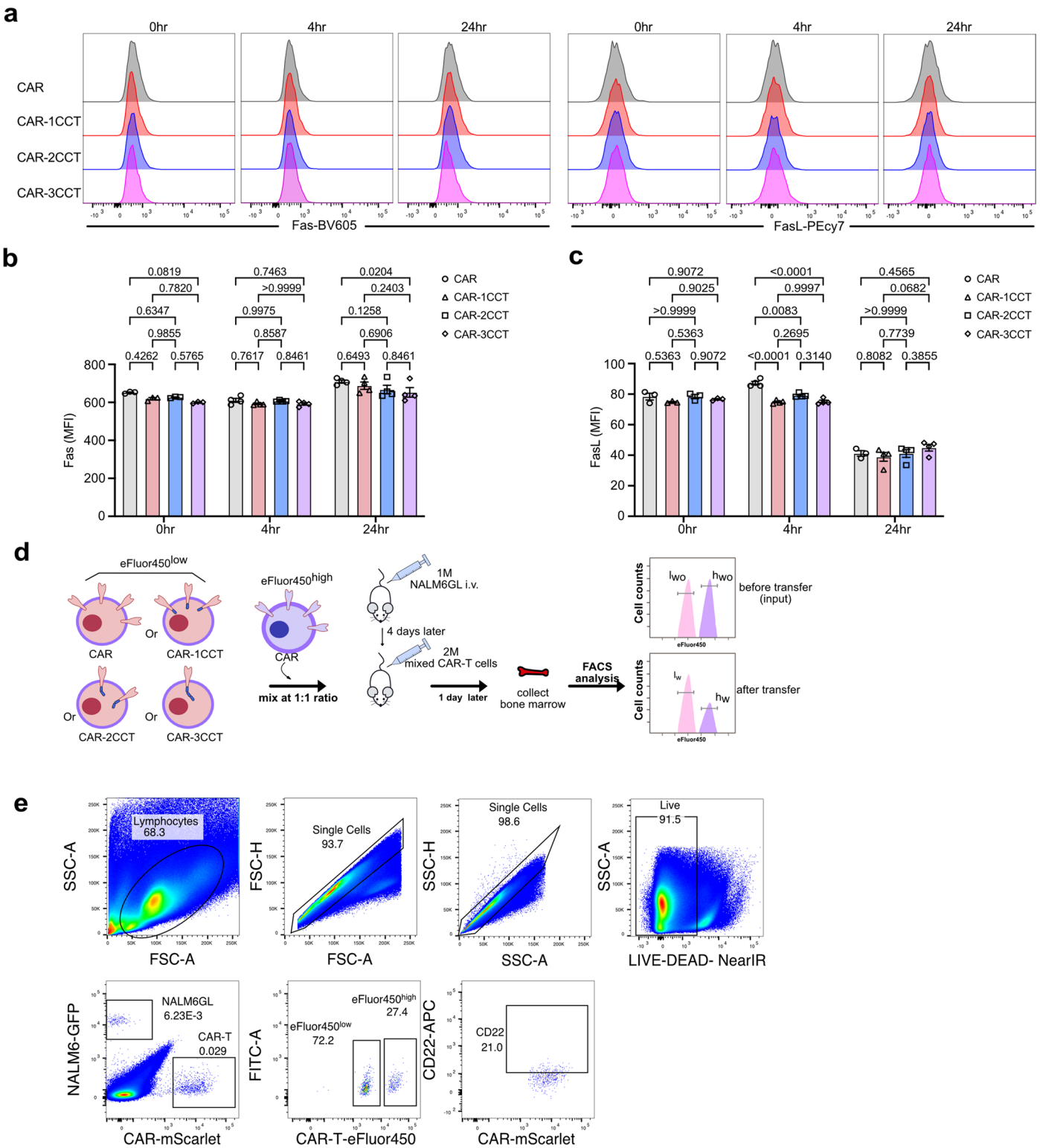

Extended Data Fig. 6 | CCT fusion enhanced CAR-T survival. a. Representative flow cytometry results showing the expression of Fas and FasL on CAR-T cells following incubations with NALM6GL cells for 0, 4 or 24 hours. **b**. Quantification of (**a**) showing the expression of Fas on CAR-T cells, n = 4. **c**. Quantification of (**a**) showing the expression of FasL on CAR-T cells, n = 4. **d**. Schematics of *in vivo* experimental workflow used in Fig. 4h–l. NSG mice (female, 6-10 weeks old) were first inoculated with 1 million NALM6GL cells intravenously (i.v.) on day 0. CAR-T cells stained with 1 μM eFluor450 were mixed with CAR-T cells stained with 10 μM eFluor450 at 1:1 ratio. Two million of these labeled cell mixtures were transferred to the leukemia NSG models on day 4. One day post CAR-T transfer, bone marrow samples were collected for flow cytometry analysis to determine the relative percentage of eFluor450^{low} and eFluor450^{high} populations. **e**. Representative flow cytometry results showing the gating strategy used in Fig. 4h–l for quantifying the relative CAR-T survival *in vivo*. For all bar plot figures, data are shown as mean ± s.e.m. Two-way ANOVA with Tukey's multiple-comparisons test is used to assess significance for (**b,c**). Exact *p* values are labeled. All numbers defined by 'n' indicate the number of biologically independent samples. Data are representative of two independent experiments performed with biological repeats.

https://doi.org/10.1038/s41590-023-01571-5

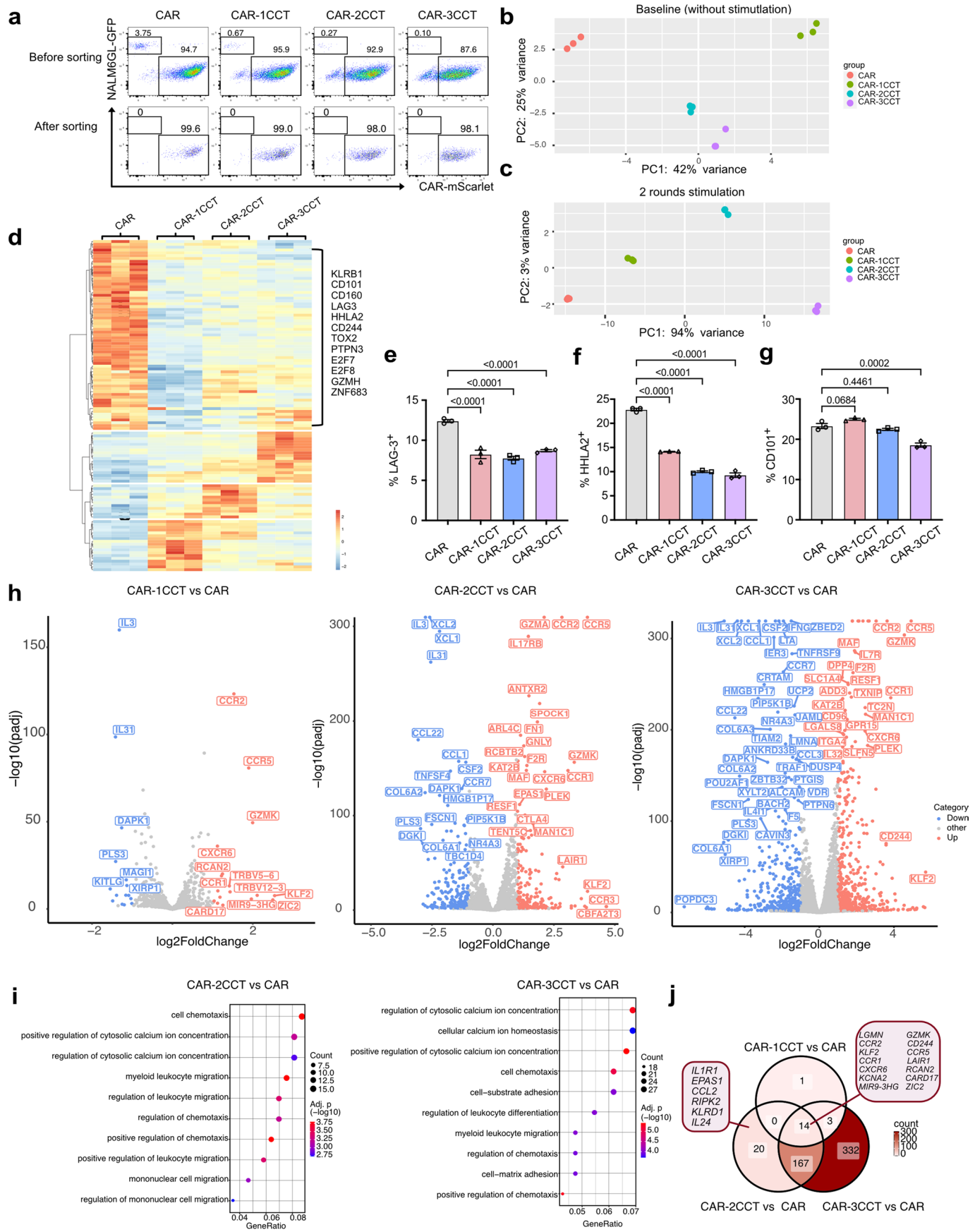

Extended Data Fig. 7 | See next page for caption.

https://doi.org/10.1038/s41590-023-01571-5

Extended Data Fig. 7 | Characterization of CAR-CCT cells by bulk RNA sequencing. a. Representative flow cytometry results showing the sorting purity of CAR-T cells before subjecting to RNA-seq. CAR-T cells after being stimulated with 2 rounds of NALM6GL cells were sorted as mScarlet^{+} GFP^{-} cells. **b**. PCA analysis of all four groups of CAR-T cells at baseline without stimulation. **c**. PCA analysis of all four groups of CAR-T cells with 2 rounds of NALM6GL stimulation. **d**. Heatmap of differentially expressed genes in all four groups of CAR-T cells at baseline. All CAR-T cells were purified by flow cytometer at day 6 after lentivirus infection and expanded for 7 days before mRNA extraction for bulk RNA sequencing. Cutoff for determining differentially expressed genes is set to be p (adj) < 0.01 and |log2Fc|> 1. **e-g**. Quantification of LAG3(**e**), HHLA2(**f**), CD101(**g**) expression level on CAR-T cells at baseline using flow cytometry, n = 3. **h**. Volcano plot of bulk RNA sequencing showing differentially expressed genes in CAR-1CCT vs. CAR (left panel), CAR-2CCT vs. CAR (middle panel) and CAR-3CCT vs. CAR (right panel). Purified CAR-T cells were co-cultured with NALM6GL cells at E/T = 1/2. NALM6GL cells were repeatedly supplemented at 24 hrs after initial co-culture. CAR-T cells (mScarlet+) were then sorted at 72 hrs after initial co-culture for bulk RNA sequencing. Cutoff for determining differentially expressed genes is set to be p (adj) < 0.01 and |log2Fc|> 1. **i**. Pathway analysis by over representation analysis (ORA) showing top 10 pathways of upregulated DEGs in CAR-2CCT vs. CAR (left panel) and in CAR-3CCT vs. CAR (right panel). **j**. Venn diagram showing overlaps of upregulated genes as in (a). For all bar plots, data are shown as mean ± s.e.m. One-way ANOVA with Dunnett's multiple-comparisons test is used to assess significance. Exact p values are labeled. All numbers defined by 'n' indicate the number of biologically independent samples. Data are representative of two independent experiments performed with biological repeats.

https://doi.org/10.1038/s41590-023-01571-5

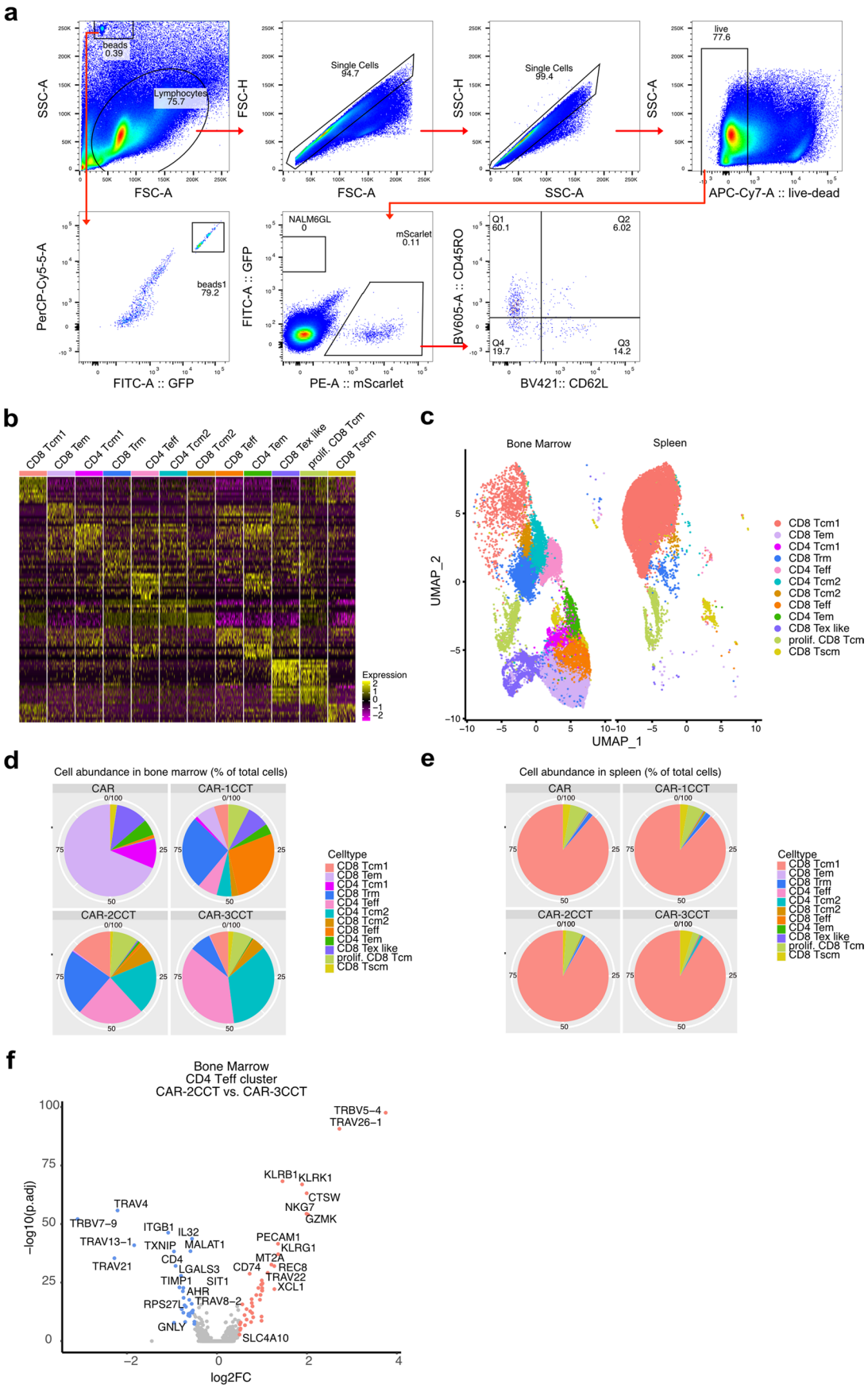

Extended Data Fig. 8 | See next page for caption.

https://doi.org/10.1038/s41590-023-01571-5

Extended Data Fig. 8 | Characterization of CAR-CCT cells in vivo via scRNA-seq. a. Gating strategy used for analysis shown in Fig. 5e–k. **b**. Heatmap showing expression profiles across 12 CAR-T cell subsets. Scaled gene expression is presented by showing 100 representative cells of each subset. **c**. UMAP visualization of 39,151 cells CAR-T cells via scRNA-seq profiling, split by tissue type. **d**. Pie chart of cell proportions between four different CAR-T groups isolated from bone marrow. **e**. Pie chart of cell proportions between four different CAR-T groups isolated from spleen. **f**. Volcano plot showing differentially expressed genes in CAR-2CCT vs. CAR-3CCT in the CD4 Teff cluster from bone marrow. Data are representative of two independent experiments performed with biological repeats.

https://doi.org/10.1038/s41590-023-01571-5

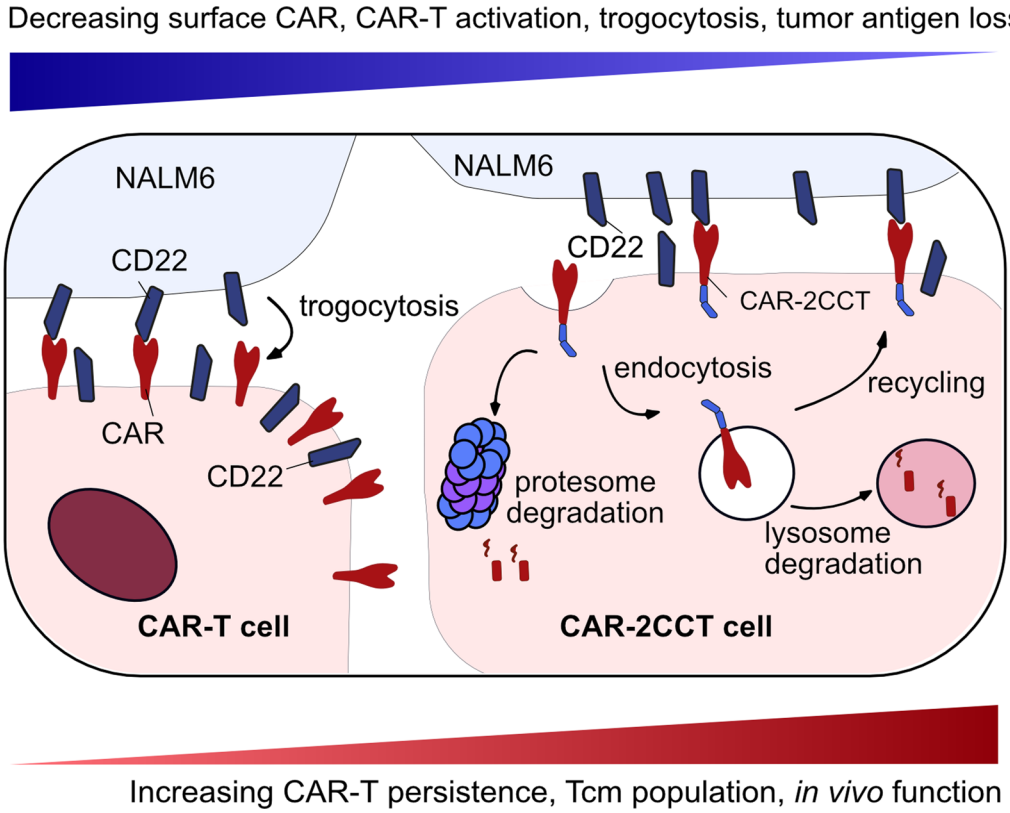

Extended Data Fig. 9 | Proposed model of titrating optimal CAR-T function with CCT fusion. CAR fused with duplex CCTs (CAR-2CCT) demonstrated decreased surface expression, which is tightly regulated by its endocytosis, recycling, degradation in both lysosome and proteasome. Compared with the control CAR, CAR-2CCT has significant decreases in surface CAR expression, T cell activation, CAR-mediated trogocytosis, and causes less tumor antigen loss on NALM6 cells. This engineering approach effectively increases the persistence and proportion of Tcm cells in CAR-2CCT cells, leading to a remarkable improvement in their anti-tumor *in vivo*.

nature portfolio

Corresponding author(s): Sidi Chen

Last updated by author(s): Jun 7, 2023

Reporting Summary

Nature Portfolio wishes to improve the reproducibility of the work that we publish. This form provides structure for consistency and transparency in reporting. For further information on Nature Portfolio policies, see our Editorial Policies and the Editorial Policy Checklist.

Statistics

For all statistical analyses, confirm that the following items are present in the figure legend, table legend, main text, or Methods section.

n/a	Confirmed	
☐	☒	The exact sample size (*n*) for each experimental group/condition, given as a discrete number and unit of measurement
☐	☒	A statement on whether measurements were taken from distinct samples or whether the same sample was measured repeatedly
☐	☒	The statistical test(s) used AND whether they are one- or two-sided *Only common tests should be described solely by name; describe more complex techniques in the Methods section.*
☒	☐	A description of all covariates tested
☐	☒	A description of any assumptions or corrections, such as tests of normality and adjustment for multiple comparisons
☐	☒	A full description of the statistical parameters including central tendency (e.g. means) or other basic estimates (e.g. regression coefficient) AND variation (e.g. standard deviation) or associated estimates of uncertainty (e.g. confidence intervals)
☐	☒	For null hypothesis testing, the test statistic (e.g. *F*, *t*, *r*) with confidence intervals, effect sizes, degrees of freedom and *P* value noted *Give P values as exact values whenever suitable.*
☒	☐	For Bayesian analysis, information on the choice of priors and Markov chain Monte Carlo settings
☒	☐	For hierarchical and complex designs, identification of the appropriate level for tests and full reporting of outcomes
☒	☐	Estimates of effect sizes (e.g. Cohen's *d*, Pearson's *r*), indicating how they were calculated

Our web collection on statistics for biologists contains articles on many of the points above.

Software and code

Policy information about availability of computer code

Data collection	Flow cytometry data was collected by BD FACSDiva™ Software v9.0; Confocal images were acquired by Leica Stellaris 8 FALCON; Bioluminescence imaging was collected by PerkinElmer Living Image v. 4.7.3; All the deep sequencing data was collected by Yale Center for Genome Analysis (YCGA).
Data analysis	Standard biological assays' data were analyzed in Prism v.8; Flow cytometry data analysis was done with FlowJo v.10.8; Multiplex cytokine measurement was analyzed by Biolegend online tool v. 2021-07-01 : https://legendplex.qognit.com/user/login?next=home Confocal images were processes and analyzed by ImageJ v.1.51; Bioluminescence imaging was analyzed by PerkinElmer Living Image v. 4.7.3; RNAseq raw data was mapped with STAR v. 2.7.9a; RNAseq data visualization was done in R v.4.0.0; Differential gene expression analysis was done with DESeq 2 v.1.28.1; Pathway analysis was done using over representation analysis (ORA) by enrichplot v.1.8.1. scRNA-seq dataset was analyzed by Cell Ranger v6.0.1 and Seurat version 4.1.1. Imaging data analysis was done with MATLAB v.R2020a. Schematic illustrations were created with Affinity Designer v. 1.10.1

For manuscripts utilizing custom algorithms or software that are central to the research but not yet described in published literature, software must be made available to editors and reviewers. We strongly encourage code deposition in a community repository (e.g. GitHub). See the Nature Portfolio guidelines for submitting code & software for further information.

Data

Policy information about availability of data

All manuscripts must include a data availability statement. This statement should provide the following information, where applicable:

- Accession codes, unique identifiers, or web links for publicly available datasets
- A description of any restrictions on data availability
- For clinical datasets or third party data, please ensure that the statement adheres to our policy

All data generated or analyzed during this study are included in this article and its supplementary information files. Specifically, source data and statistics for non-high-throughput experiments such as flow cytometry or cellular assays are provided in an excel file of Source data and statistics (Supplementary Table 3). Processed data for genomic sequencing (e.g. RNA-seq and scRNA-seq) and other forms of high-throughput experiments are provided as processed quantifications in Supplementary Table 1 and 2. Genomic sequencing raw data are deposited to Gene Expression Omnibus (GEO), with accession numbers: GSE234307. The code used for data analysis and the generation of figures related to this study can be accessed from GitHub with this link: https://github.com/Ariel-Xiaoyu/CAR-CCT. The customized MATLAB (Mathworks, Natick, MA) App used for image analysis is available at: https://github.com/xs254/Colocalization_calculator/tree/main.

Field-specific reporting

Please select the one below that is the best fit for your research. If you are not sure, read the appropriate sections before making your selection.

☒ Life sciences ☐ Behavioural & social sciences ☐ Ecological, evolutionary & environmental sciences

For a reference copy of the document with all sections, see nature.com/documents/nr-reporting-summary-flat.pdf

Life sciences study design

All studies must disclose on these points even when the disclosure is negative.

Sample size	Sample size was determined according to the lab's prior work or similar approaches in the field (Hamieh, M. et al. CAR T cell trogocytosis and cooperative killing regulate tumour antigen escape. (2019) Nature 568, 112-116, doi:10.1038/s41586-019-1054-1).
Data exclusions	No data were excluded.
Replication	Number of biological replicates are indicated in the figure legends. For all experiments, the findings were replicated in at least two independent repeats.
Randomization	PBMCs used for CAR-T generation were randomized by patient sex and age. For in vivo studies, Individual mouse was randomized by littermates and cages.
Blinding	Whenever possible, investigators are blinded for acquisition and analysis of data. In vitro CAR-T killing assay experiments and Quantification of images were blinded by anonymized labeling. In such experiments, the group identity is unknown to data collector/analyst. Other experiments are not blinded, as it did not affect reproducibility.

Reporting for specific materials, systems and methods

We require information from authors about some types of materials, experimental systems and methods used in many studies. Here, indicate whether each material, system or method listed is relevant to your study. If you are not sure if a list item applies to your research, read the appropriate section before selecting a response.

Materials & experimental systems

n/a	Involved in the study
☐	☒ Antibodies
☐	☒ Eukaryotic cell lines
☒	☐ Palaeontology and archaeology
☐	☒ Animals and other organisms
☒	☐ Human research participants
☒	☐ Clinical data
☒	☐ Dual use research of concern

Methods

n/a	Involved in the study
☒	☐ ChIP-seq
☐	☒ Flow cytometry
☒	☐ MRI-based neuroimaging

Antibodies

Antibodies used	Phospho-ERK1/2 (Thr202, Tyr204) Monoclonal Antibody;eBioscience; Clone: OKT3; Catalog number:17-9109-42 Alexa Fluor® 647 anti-human CD3 Antibody; BioLegend; Clone:OKT3; Catalog number:317312 Alexa Fluor® 647 anti-human CD19 Antibody; BioLegend; Clone:A17136C; Catalog number:396304

Alexa Fluor® 647 anti-rat IgG2a Antibody; BioLegend; Clone:MRG2a-83; Catalog number:407512
FITC anti-human CD45RA Antibody; BioLegend; Clone:HI100 ; Catalog number:304106
APC anti-human CD152 (CTLA-4) Antibody; Biolegend; Clone:BNI3; Catalog number:369612
APC anti-human CD107a (LAMP-1) Antibody; BioLegend; Clone:H4A3 ; Catalog number:328620
APC anti-human CD4 Antibody; BioLegend; Clone:A161A1; Catalog number:357408
APC anti-human CD19 Antibody; BioLegend; Clone:4G7; Catalog number:392504
APC anti-human CD22 Antibody; BioLegend; Clone:S-HCL-1 ; Catalog number:363506
APC anti-human CD279 (PD-1) Antibody; BioLegend; Clone:EH12.2H7; Catalog number:329908
APC anti-human IFN-γ Antibody; BioLegend; Clone:B27; Catalog number:506510
Brilliant Violet 605™ anti-human CD3 Antibody; BioLegend; Clone:OKT3; Catalog number:317322
Brilliant Violet 421™ anti-human CD8 Antibody; BioLegend; Clone:SK1; Catalog number:344748
Brilliant Violet 605™ anti-human CD45RO Antibody; BioLegend; Clone:UCHL1; Catalog number:304238
Brilliant Violet 605™ anti-human CD95 (Fas) Antibody; BioLegend; Clone:DX2; Catalog number:305627
Brilliant Violet 421™ anti-human CD62L Antibody; BioLegend; Clone:DREG-56; Catalog number:304828
Brilliant Violet 421™ anti-human CD279 (PD-1) Antibody; BioLegend; Clone:EH12.2H7; Catalog number:329919
Brilliant Violet 421™ anti-human IgG Fc Antibody; BioLegend; Clone:HP6017; Catalog number:409318
Brilliant Violet 421™ anti-human TNF-α Antibody; BioLegend; Clone:MAb11; Catalog number:502932
Brilliant Violet 421™ anti-DYKDDDDK Tag Antibody; BioLegend; Clone:L5; Catalog number:637322
PerCP/Cyanine5.5 anti-human CD366 (Tim-3) Antibody; BioLegend; Clone:F38-2E2; Catalog number:345016
PerCP/Cyanine5.5 anti-human Perforin Antibody; BioLegend; Clone:dG9; Catalog number:308114
PerCP/Cyanine5.5 anti-human TIGIT (VSTM3) Antibody; BioLegend; Clone:A15153G; Catalog number:372718
PE/Cyanine7 anti-human CD178 (Fas-L) Antibody; BioLegend; Clone:NOK-1; Catalog number:306417
PE/Cyanine7 anti-human CD3 Antibody; BioLegend; Clone:OKT3; Catalog number:317334
PE/Cyanine7 anti-human CD223 (LAG-3) Antibody; BioLegend; Clone:11C3C65; Catalog number:369310
PE anti-human IgG Fc Antibody; BioLegend; Clone:HP6017; Catalog number:409304
Brilliant Violet 421™ anti-human CD244 (2B4) Antibody; biolegend; Clone:2-69; Catalog number:393503
PerCP/Cyanine5.5 anti-human CD160 Antibody; biolegend; Clone:BY55; Catalog number:341209
APC anti-human CD101 (BB27) Antibody; biolegend; Clone:BB27; Catalog number:331007
B7-H7(HHLA2) Monoclonal Antibody (MA57YW), PE-Cyanine7, eBioscience™; Thermo; Clone:MA57YW; Catalog number:25-6537-41
Unless specified otherwise in the Methods section, all antibodies used for flow cytometry is diluted 1: 200

Validation

Antibodies were validated by the vendors by staining cell line overexpressing target antigen or primary immune cells under different stimuli using flow cytometry or immunohistochemistry.

Eukaryotic cell lines

Policy information about cell lines

Cell line source(s)

293T; ATCC; Catalog Number : CRL-3216
NALM6; ATCC; Catalog Number : CRL-3273
Jurkat; ATCC; Catalog Number : TIB-152
NALM6GL (Dai X, Park J J, Du Y, et al. One-step generation of modular CAR-T cells with AAV–Cpf1[J]. Nature methods, 2019, 16(3): 247-254.)
Human Peripheral Blood Mononuclear Cells; STEMCELL; Catalog Number : 70025.1

Authentication

All cell lines used have been authenticated by the original vendors. Cell line from ATCC have been tested and authenticated using morphology, STR profiling, karyotyping and PCR approaches to confirm the identity of cell lines. NALM6, Jurkat and Human T cells were validated by investigators based on surface expression of CD22, CD3, CD4,or CD8 using flow cytometry.

Mycoplasma contamination

All cell lines tested negative for mycoplasma contamination.

Commonly misidentified lines
(See ICLAC register)

No misidenified cell lines were used in the study.

Animals and other organisms

Policy information about studies involving animals; ARRIVE guidelines recommended for reporting animal research

Laboratory animals

NOD.Cg-Prkdcscid Il2rgtm1Wjl/SzJ (NSG) mice were purchased from the Jackson Laboratory and bred in-house. Both male and female NSG mice between 6 to 8 weeks old were used. Mice were housed in standard vivarium condition at YARC, with free access to water and food, ambient room temperature (approximately 22 degree Celsius) and humidity-controlled. Mice were maintained on a 14h:10h light/dark cycle (07:00 to 21:00 light on). Mouse health checks were performed regularly.

Wild animals

No wild animals were used in this study.

Field-collected samples

No field collected samples were used in the study.

Ethics oversight

All animal work was approved by Yale University's Institutional Animal Care and Use Committee (IACUC) and performed with approved protocols (#2018-20068; #2021-20068).

Note that full information on the approval of the study protocol must also be provided in the manuscript.

Flow Cytometry

Plots

Confirm that:

☒ The axis labels state the marker and fluorochrome used (e.g. CD4-FITC).

☒ The axis scales are clearly visible. Include numbers along axes only for bottom left plot of group (a 'group' is an analysis of identical markers).

☒ All plots are contour plots with outliers or pseudocolor plots.

☒ A numerical value for number of cells or percentage (with statistics) is provided.

Methodology

Sample preparation	Cell surface antigens were stained with indicated antibody cocktails in MACS buffer on ice for 15 minutes or 1 hour as indicated in the figure legend.
Instrument	Flow cytometric analysis was performed on an BD FACSAria II
Software	FlowJo v.10.8 was used for flow ctyometry data analysis.
Cell population abundance	For CAR-T cells sorting, sorting purity was checked after every sort to make sure it is higher than 95%.
Gating strategy	A lymphocyte gate was defined first from FSC-A v SSC-A. Singlet gates were then defined on FSC-H vs FSC-A. Dead cells were excluded by live/dead staining. Additional gating was performed as described in figures.

☒ Tick this box to confirm that a figure exemplifying the gating strategy is provided in the Supplementary Information.